

# A one-dimensional temperature and age modeling study for selecting the drill site of the oldest ice core ~~around~~near Dome Fuji, Antarctica

Takashi Obase<sup>1</sup>, Ayako Abe-Ouchi<sup>1,2</sup>~~Ouchi~~<sup>1,2</sup>, Fuyuki Saito<sup>3</sup>, Shun ~~Tsutaki~~<sup>2,4</sup>Tsutaki<sup>2,4</sup>, Shuji ~~Fujita~~<sup>2,4</sup>Fujita<sup>2,4</sup>, Kenji Kawamura<sup>2,3,4</sup> and Hideaki ~~Motoyama~~<sup>2,4</sup>Motoyama<sup>2,4</sup>

<sup>1</sup> Atmosphere and Ocean Research Institute, The University of Tokyo, Kashiwa, Japan

<sup>2</sup> National Institute of Polar Research, Research Organization of Information and Systems, Tachikawa, Japan

<sup>3</sup> Japan Agency for Marine-Earth Science and Technology (JAMSTEC), Yokosuka, Japan

<sup>4</sup> The Graduate University for Advanced Studies, SOKENDAI, Tachikawa, Japan

Correspondence to: Takashi Obase (obase@aori.u-tokyo.ac.jp)

**Abstract.** The recovery of a new Antarctic ice core spanning the ~~last~~past ~1.5 million years will advance our understanding of climate system dynamics during the Quaternary. ~~Recent~~Recently, glaciological field surveys have been conducted to select the most suitable core location near Dome Fuji (DF), Antarctica. Specifically, ground-based radar-echo soundings have been used to acquire highly detailed images of bedrock topography and internal ice layers. In this study, we use a one-dimensional (1-D) ice flow model to compute the temporal evolutions of age and temperature, in which the ice flow is linked with not only transient climate forcing associated with past glacial–interglacial cycles, but also transient basal melting diagnosed along the evolving temperature profile. We investigated the influence of ice thickness, accumulation rate, and geothermal heat flux on the age and temperature profiles. The model was constrained by the observed temperature and age profiles reconstructed from DF ice-core analysis. The results of sensitivity experiments indicate that ice thickness is the most crucial parameter influencing the computed age of the ice because it is critical to the history of basal temperature and basal melting, which can eliminate old ice. The 1-D model was applied to a 54 km-~~l~~ong transect in the vicinity of DF and compared with radargram data. We found that the basal age of the ice is mostly controlled by the local ice thickness, demonstrating the importance of high spatial resolution surveys of bedrock topography for selecting ice-core drilling sites.

## 1. Introduction

Earth’s climate system experienced glacial–interglacial cycles during the Quaternary, associated with the waxing and waning of continental ice sheets and climate system feedbacks- (e.g., Shakun et al., 2015). Ice cores from the Antarctic ice sheet have provided fruitful information on past climate system changes-~~in the past~~ because they can provide continuous reconstructions of ~~past~~ atmospheric compositions and temperature up to ~800 thousand years before the present (ka BP) (Jouzel et al., 2007; Kawamura et al., 2017). Such reconstructions have contributed to our understanding of the climate system dynamics of glacial–interglacial cycles (e.g., Abe-Ouchi et al., 2013; Obase et al., 2021). Meanwhile, a stacked sequence of marine sediments (Lisiecki and Raymo, 2005) indicates that the periodicity of glacial–interglacial cycles changed from 40 to 100 ka at the middle Pleistocene transition (MPT, approximately 800–1250 ka BP, Paillard, 2001; Clark et al., 2006). However, continuous ice core records that cover the MPT are still lacking, leading to a limited understanding of the mechanisms of this climate event. To help remedy this issue, the International Partnership for Ice Core Sciences (IPICS) has identified the quest for an “oldest ice core” as a critically~~critical~~ scientific ~~challenges~~challenge. In this article, we define the term “old ice” as a continuous ice core with a basal age reaching 1.5 million years (Ma) BP, as defined in a IPICS community paper (Fischer et al., 2013).

In recent years, international efforts have been made to find plausible sites to obtain old ice in several locations in the interior of the Antarctic continent. In particular, in EPICA (European Project for Ice Coring in Antarctica) Dome C (EDC), glaciological surveys and ice-flow modeling studies

48 have been used to select the location of ~~the~~ suitable sites (Parrenin et al., 2017; Young et al., 2017;  
49 Passalacqua et al., 2018; Lilien et al., 2021). The present article focuses on Dome Fuji (DF), Antarctica,  
50 which is located at 77.31° S, 39.70° E, with a surface elevation of 3810 m above sea level, and ice  
51 thickness of 3028 m. The most recent ice core at DF was obtained between 2003 and 2006 (Motoyama  
52 et al., 2021). The ice age at the bottom of this core was approximately 720 ka BP based on Antarctic  
53 ice core chronology 2012 (AICC2012) (Kawamura et al., 2017; Uemura et al., 2018). The temperature  
54 of the ice was at the pressure-melting point near the bedrock (Motoyama et al., 2021). Recently, field  
55 surveys have been conducted to collect bedrock elevation data near DF using ground and airborne  
56 radar surveys. On the basis of surveys performed by Japanese Antarctic Research Expeditions (JARE)  
57 ~~since~~between the late 1980s ~~until~~and 2008, the results of which are included in BEDMAP2 datasets  
58 (Fretwell et al., 2013), the typical ice thickness around DF is approximately 2000–3200 m (Fig. 1).  
59 ~~Later~~Subsequently, the 54th JARE (2012–2013 Antarctic summer) conducted ground-based radar  
60 surveys in areas where subglacial mountains were detected in the area south of DF (data compiled in  
61 Tsutaki et al., 2022). More recently, the Alfred Wegener Institute (AWI) in Germany conducted  
62 airborne radar surveys covering the DF area (Karlsson et al., 2018). ~~Based on~~On the basis of these data,  
63 the 59th and 60th JARE (2017–2018 and 2018–2019 Antarctic summers) conducted ground radar  
64 surveys to investigate the internal layers of ice sheets over ~~an areal extent a~~ distance of ~ 505650 km,  
65 (Tsutaki et al. 2022), covering the DF and NDF sites (the latter located at 77.8° S, 39.05° E, south of  
66 DF) (Rodriguez-Morales et al., 2020).

67 To select suitable ice-core drilling sites, ~~it is essential to investigate~~ the conditions that are  
68 required to preserve old ice using constraints from glaciological and climatological data should be  
69 investigated. Previous ice-flow modeling studies have examined the requirements to preserve old ice  
70 using both three-dimensional (3-D) and one-dimensional (1-D) models. Pattyn (2010) used a 3-D ice  
71 sheet model under present-day constant climate forcing, and suggested the importance of minimal  
72 horizontal flow and low geothermal heat flux (GHF) to preserve old ice near the base of ice sheets.  
73 Other studies have used 3-D models to represent 3-D ice-flow fields and ice age for the relatively small  
74 area near Antarctic Domes (Huybrechts et al., 2007; Seddik et al., 2011; Sun et al., 2014; Passalacqua  
75 et al., 2018; Zhao et al., 2018). These studies estimated the age distribution of the ice expected from  
76 3-D ice flow fields under a constant present-day climate. More recent studies used glacial–interglacial  
77 cycle forcing (Sutter et al., 2019, 2021) and discussed how the past variation of the Antarctic ice sheet  
78 affects ice age distributions.

79 One-dimensional vertical ice-flow models have been used as the vertical profiles of age and  
80 temperature near Antarctic Domes, where horizontal flow is relatively minor. Horizontal surface  
81 velocity in the vicinity of DF and NDF is  $< 2 \text{ m a}^{-1}$ , and it has minor spatial variations, evidenced by  
82 satellite-based measurements (Rignot et al., 2011, 2017; Mouginot et al., 2012). Such 1-D models  
83 perform well in long-term forward simulations over glacial cycles and are able to conduct many  
84 ~~experimentssimulations~~ simulations with different parameters. In particular, Fischer et al. (2013) investigated the  
85 influence of a wide range of parameters, including ice thickness, accumulation, and GHF on the basal  
86 age of ice. ~~The~~Their key finding was that melting at the base reduces the likelihood of old ice; ~~hence,~~  
87 ~~a lower accumulation rate~~, and a lower ice thickness ~~compared with~~ than that at previous ice core sites  
88 ~~are~~ a required ~~conditions~~ condition to avoid basal melting ~~and preserve old~~. Furthermore, a lower  
89 accumulation rate generally contributes to increasing the age of the ice at a certain height from the  
90 bedrock but increases the chance of basal melting, owing to the reduced vertical advection of cold ice.  
91 Other studies used an equivalent 1-D ice-flow model, investigated the necessary conditions to keep the  
92 ice base frozen (Van Liefferinge and Pattyn, 2013; Van Liefferinge et al., 2018), and examined the  
93 observed basal conditions of the ice (Passalacqua et al., 2017). Parrenin et al. (2017) estimated ice-  
94 flow parameters and basal melting rate using internal layers of the ice near EDC and proposed  
95 candidate sites for old ice. Saito et al. (2020) presented a numerical scheme of ice advection calculation  
96 and conducted numerical simulations using idealized glacial cycle forcings. This contributed to a good  
97 representation of annual layer thickness, which is critical to the occurrence of old ice near the base of

98 ~~the~~ ice column.

99 Simplified factors in previous modeling studies were the time-dependent climate forcing and  
100 temperature profile, which are critical to basal ice melting. In particular, the basal temperature of the  
101 ice sheet shows a minimum during interglacials because it takes a long time to ~~convey the information~~  
102 ~~of~~ ~~advect and diffuse~~ surface temperature changes to the base of the ice sheet (Saito and Abe-Ouchi,  
103 2004; Van Liefferinge et al., 2018). In this context, the model used in Parrenin et al. (2007, 2017)  
104 assumed that basal melting rates were constant over time, and Fischer et al. (2013) used a constant  
105 climate forcing. Parrenin et al. (2017) assumed that the temporal variations in basal melting rates are  
106 the same as accumulation rates. Some studies (Van Liefferinge and Pattyn, 2013; Passalacqua et al.,  
107 2017; Van Liefferinge et al., 2018) have investigated ice temperature using realistic climate forcing,  
108 but did not investigate the resultant impact on the age of the ice. Similarly, Hondoh et al. (2002) and  
109 Talalay et al. (2021) estimated GHF at DF and other Antarctic domes based on observed vertical  
110 temperature profiles, but the observed age–depth profiles were not used as constraints. The ice  
111 thickness at Antarctic domes also changes with time, and can be up to 150 m thinner during glacial  
112 periods when surface mass balance (SMB) is reduced (Saito and Abe-Ouchi, 2010).

113 Despite the close link between the temperature and age of ice owing to basal melting, the  
114 coupled simulations of thermodynamics and age of ice ~~and time-dependent basal melting~~ were not  
115 represented under transient climate forcing in previous modeling studies of old ice. In this study, we  
116 use a 1-D ice-flow model, which simultaneously computes the evolution of ice temperature and age,  
117 and the model is forced by past climate history. The remainder of the article is organized as follows:  
118 Section 2 describes the 1-D model used in this study. In Sect. 3, we apply this model to DF and conduct  
119 systematic sensitivity experiments to calibrate GHF and a tuning parameter of the vertical profile of  
120 ice velocity by comparing simulated age and temperature profiles with observations. We also use  
121 parameters at EDC to examine whether the model can simulate temperature and age profiles under  
122 different glaciological conditions. In Sect. 4, using the results of the tuned vertical velocity parameters,  
123 we investigate the influences of ice thickness, ~~surface mass balance (SMB), SMB,~~ and GHF on the  
124 basal temperature and age. In Sect. 5, we apply the 1-D model to the DF–NDF transect (over a distance  
125 of ~ 50 km) and compare the results with the internal layers of the ice.

## 127 2. Method

### 128 2.1. Model description

129 We used a 1-D ice-flow model, Icies-2 (Saito et al., 2020). This model computes the temporal  
130 evolutions of the age and temperature profiles of ice columns.

131 The evolution of the age of the ice is computed using the vertical advection equation,

$$132 \frac{\partial A}{\partial t} = -w \frac{\partial A}{\partial z} + 1, \quad (1)$$

133 where  $A$  is the age of the ice, defined as the duration since deposition, and  $w$  is the vertical velocity of  
134 the ice (a positive value indicates upward velocity). Here,  $\zeta$  is a normalized coordinate defined as  $\zeta =$   
135  $\frac{s-z}{H}$ , where  $s$  is the surface elevation,  $z$  is the height above bedrock, and  $H$  is the ice thickness (thus  
136  $\zeta = 1$  and  $0$  correspond to the ice surface and base, respectively). The first and second terms on the  
137 right-hand side of Equation (1) represent the vertical advection and aging owing to time-lapse,  
138 respectively.

139 The vertical velocity of the ice ~~can~~ is assumed to be represented as:

$$140 w(\zeta) = - \left[ \left( M_s + M_b - \frac{\partial H}{\partial t} \right) \omega(\zeta) - M_b \right], \quad (2)$$

141 ~~where~~ the terms  $M_s$  and  $M_b$  represent surface (positive indicates ice gain) and basal  
142 (~~positive~~ negative indicates ice melt) mass balance caused by accumulation and ~~ablation~~ basal melting,  
143 respectively, and  $\frac{\partial H}{\partial t}$  is the change in ice thickness over time. The normalized vertical velocity profile,  
144  $\omega$ , is given as a function of the normalized coordinate following previous studies (Van Liefferinge and  
145 Pattyn, 2013; Passalacqua et al., 2017; Van Liefferinge et al., 2018), and derived from derived from

Parrenin and Hindmarsh (2007), and Llibourey (1979):

$$\omega(\zeta) = 1 - \frac{p+2}{p+1}(1 - \zeta) + \frac{1}{p+1}(1 - \zeta)^{p+2}, \quad (3)$$

where  $\omega$  is 1 at the surface and 0 at the base. Hence, ~~if we assume in the case of~~ steady state,  $\frac{\partial H}{\partial t} = 0$ , the vertical velocity of the ice at the surface and base equates to  $-M_s$  and  $M_b$ , respectively. The shape of  $\omega$  with different  $p$  parameters is ~~shown demonstrated~~ in Fig. 2, indicating that a larger  $p$ -value ~~tends to induce yields~~ a larger downward ice velocity. Compared with Fischer et al. (2013), ~~in the case of who used a different formulation of the vertical velocity profile with an  $m$  parameter (similar role as  $p$  of this study) of  $m = 0.5$  in their study~~ (Fig. 2 dashed lines),  $p = 3$  from Equation (3) gives a different vertical temperature profile, with a smaller vertical velocity, particularly near the base of the ice.

The temperature of the ice is computed using the following vertical advection and diffusion equation:

$$\frac{\partial T}{\partial t} = -w \frac{\partial T}{\partial z} + \frac{1}{\rho_I c_p} \frac{\partial}{\partial z} \left( \kappa \frac{\partial T}{\partial z} \right), \quad (4)$$

~~where where  $T$  is the temperature of the ice [K],  $\kappa$  is the thermal conductivity,  $\rho_I$  is the ice density, and  $c_p$  is the heat capacity of the ice. The density of ice is set as a constant ( $910 \text{ kg m}^{-2}$ ), i.e., we ignore the effects of lower density in the firn column. The strain heating term is neglected in the present study, given that deformation of the ice would be minor near Antarctic domes because of very low horizontal shear. The thermal conductivity and specific heat capacity of the ice are functions of temperature (Greve and Blatter, 2009, following Ritz, 1987). The density of ice is set as a constant ( $910 \text{ kg m}^{-2}$ ), i.e. we ignore effects of lower density in the firn column.):~~

$$\kappa = 9.828e^{-0.0057T} \text{ W m}^{-1} \text{ K}^{-1} \quad (5)$$

$$c_p = (146.3 + 7.253T) \text{ J kg}^{-1} \text{ K}^{-1} \quad (6)$$

Boundary conditions at the surface and base of the ice are required to close the equations. At the ice surface, the age is set as 0, assuming no surface melt, and the temperature is set to the surface temperature at the given time. The basal boundary conditions for temperature depend on the basal condition:

$$\frac{\partial T}{\partial z} \Big|_b = -\frac{G}{\kappa} \text{ if no melting,} \quad (57)$$

$$T_b = T_{pm} \text{ if melting,} \quad (68)$$

where  $G$  is the geothermal heat flux (GHF) at the ice–bedrock boundary, and  $T_{pm}$  is the pressure-melting point of the ice, which is given as a function of depth using a Clausius–Clapeyron gradient ( $8.7 \times 10^{-4} \text{ K m}^{-1}$ ). The basal melting rate at the ice–bedrock interface is determined by the conservation of heat:

$$M_b \rho_I L = G - \kappa \frac{\partial T}{\partial z}, \quad (79)$$

where  $L$  is the latent heat of the ice ( $335,000 \text{ J kJ kg}^{-1}$ ), and  $\frac{\partial T}{\partial z} \Big|_b$  is the temperature gradient at the ice–bedrock interface. This model assumes basal melting only occurs at ice–bedrock interfaces, and the temperature gradient at the ice–bedrock interface is calculated using a ~~central one-sided~~ difference discretization. The calculated basal melting rate  $M_b$  influences the velocity field according to Equation (2). ~~Basal melting can occur in the interior of the ice as represented by polythermal ice sheet models, but we ignore such effects in this study for simplicity. For this reason, we set the vertical resolution of the model for thermodynamics as relatively coarse ( $\sim 30 \text{ m}$ ) to prevent representing layers of basal melting, which can have significant errors in the diagnosis of basal melting rates. The model in the present study forecasts temperature in the bedrock, and thus the GHF at the ice–bedrock interface has temporal variations. The bedrock is 3000 m thick divided vertically into 17 equal layers; constant physical parameters are used for the bedrock (density =  $2700.0 \text{ kg m}^{-3}$ , heat capacity =  $1000.0 \text{ J kg}^{-1} \text{ K}^{-1}$ , and heat conductivity =  $3.0 \text{ W m}^{-1} \text{ K}^{-1}$ ).~~

We adopted different vertical resolution setups in computations of the temperature and age of the ice. The ice profile was discretized with 101 even vertical layers for thermodynamics; it was

192 discretized with 2661 unevenly spaced vertical layers (finer near the base to resolve the thin layers of  
 193 old ice) for age calculations, which was optimized following Saito et al. (2020). In the typical ice  
 194 column thickness of 3000 m near DF, the vertical resolution was set to approximately 20 m near the  
 195 surface and 20 cm near the bedrock, which is sufficient to resolve paleoclimate information (glacial–  
 196 interglacial annual layer variations) of ~1 ka. We used the rational function-based constrained  
 197 interpolation profile (RCIP) scheme in the advection equation for the numerical scheme, as in Saito et  
 198 al. (2020). One significant advantage of this scheme is the avoidance of numerical diffusion and ability  
 199 to reasonably preserve the time derivative of age, which is critical to the resolution of old ice. ~~The time  
 200 step was set to 5 years, and the basal melting rates were updated every 500 years to reduce the effect  
 201 of temporal oscillations in basal melting and freezing.~~ We have tested the sensitivity to the vertical  
 202 resolution of temperature calculation and found that using fine vertical resolution leads to the formation  
 203 of a temperature inversion layer in the bottom of the ice, which can be a significant error in estimating  
 204 basal temperature gradient and basal melting. Therefore, we set the number of vertical layers of the  
 205 model for thermodynamics as 100 (each approximately 30 m thick) to prevent the representation of  
 206 temperature inversion layers. The time steps of the calculation of temperature and age were set to 20  
 207 years.

### 3. Model calibration using DF age and temperature profiles

#### 3.1. Experimental design

211 This section applies the 1-D model to DF under a realistic climate history for model calibration  
 212 and parameter ~~constraints~~ constraint. Parrenin et al. (2007) determined the  $p$ -value as ~3.7 for DF, but  
 213 the chronology of ice older than 335 ka BP was not established at that time; therefore, we revisited DF  
 214 to determine the  $p$ -value covering the entire DF ice core age–depth dataset. The glaciological boundary  
 215 conditions at DF are summarized in Table 1: we used an ice thickness of 3028 m, a present-day SMB  
 216 of 30 ice equivalent mm a<sup>-1</sup> (equivalent to 27.3 freshwater mm a<sup>-1</sup>, based on Kameda et al., 2008 and  
 217 Fujita et al., 2011), and ~~-55.5 °C for the~~ mean ice surface temperature at present of -55.5 °C. We  
 218 determined the boundary condition of ice surface temperature by calibrating the temperature profile to  
 219 be consistent with measured temperature profiles of the top 500 m of the ice, within uncertainty ranges  
 220 of the observations. The observed present-day 10-m-depth annual mean snow temperature is -57.3 °C  
 221 (Kameda et al., 1997), which was also used in Parrenin et al. (2007). We note that the annual mean  
 222 surface air temperature (SAT) based on meteorological ~~observation~~ observations was -54.4 °C (during  
 223 the period 1995–1997, (Yamanouchi et al., 2003).

224 The model was forced by a realistic history of SAT (~~surface air temperature~~) and SMB. We  
 225 used local SAT anomalies at DF for the past 715 ka BP (Uemura et al., 2018) and the benthic record  
 226 of marine oxygen isotope data (Lisiecki and Raymo, 2005) to construct a continuous time series of  
 227 SAT anomalies during the last 2 Ma. We applied a simple translation of  $\delta^{18}\text{O}$  to scale the temperature  
 228 change at DF by the amplitude of glacial–interglacial cycles:

$$\Delta T_s = \alpha(\beta - \delta^{18}\text{O}) \quad (8), \quad (10)$$

230 where  $\delta^{18}\text{O}$  is the benthic marine oxygen isotope value [‰]; we set  $\alpha = 4.5$ , and  $\beta = 3.23$   
 231 to scale the amplitude of the glacial cycles, which generated a time series of temperature change over  
 232 the last 2 Ma, as shown in Fig. 3a. We used past SMB as a function of temperature anomaly compared  
 233 with the present day following Huybrechts and Oerlemans (1990), ~~as used in paleoclimate 3-D  
 234 Antarctic ice sheet modeling (Saito and Abe-Ouchi 2010), which is based on saturation vapor pressure:~~

$$\text{SMB}(t) = \text{SMB}(\text{ref}) \cdot \exp\left\{22.47\left[\frac{T_0}{T_f(\text{ref})} - \frac{T_0}{T_f(t)}\right]\right\} \left\{\frac{T_f(\text{ref})}{T_f(t)}\right\}^2 \quad (11)$$

236 where  $\text{SMB}(t)$  and  $\text{SMB}(\text{ref})$  represents past and present SMB, respectively.  $T_0 = 273.16$  K is  
 237 the triple point of water, and  $T_f$  is the atmospheric temperature above the inversion layer as a function  
 238 of surface temperature ( $T_f$  [K] =  $0.67T_s$  [K] + 88.9). From this function, an increase in surface air  
 239 temperature of 1 °C increases SMB by approximately 7% (Fig. 3b). At the Last Glacial Maximum  
 240 (LGM, approximately 20 ka BP), when SAT was 8 °C cooler, the SMB was approximately 60% of

241 ~~that of~~ the present day (Fig. 3b), which is consistent with reconstructions based on the isotopic content  
242 of the ice (Parrenin et al., 2016). This relationship between SAT and precipitation changes used ~~in this~~  
243 ~~study herein~~ was within uncertainties estimated from observations and climate model simulations,  
244 following a summary by IPCC AR6 ~~in~~ (Chapter 9.4.2.3-; Fox-Kemper et al., 2021), which used the  
245 studies of Bracegirdle et al. (2020) and Frieler et al. (2015). Although this relationship is not based on  
246 SMB, but rather on precipitation, herein we assume the precipitation change ratio is the same as that  
247 of the SMB. The other boundary conditions (ice thickness and GHF) were set as constants in the  
248 present study. ~~Some modeling studies have considered ice thickness changes over glacial cycles~~  
249 ~~because it can change by approximately 200 m (Parrenin et al., 2007), but herein, the ice thickness is~~  
250 ~~fixed, and the ice thickness tendency is assumed to be 0. One recent study (Buizert et al., 2021)~~  
251 ~~proposed that the temperature change at the LGM in interior regions of the East Antarctic ice sheet~~  
252 ~~was less than previously estimated. Therefore, we conducted one set of experiments where SAT~~  
253 ~~anomalies were set to 0%, 25%, 50%, and 75% of the standard experiments, while keeping changes in~~  
254 ~~SMB the same. Furthermore, we also applied this model to the conditions at EDC to check whether~~  
255 ~~the model could simulate observed temperature and age profiles (Table 1).~~

256 We used a result of transient simulation obtained by a 3-D ice sheet model to simulate past  
257 ice thickness history; we used the 3-D ice sheet model IcIES, which computes dynamics and  
258 thermodynamics of ice sheets using the shallow-ice approximation. The experimental design was  
259 similar to that of Saito and Abe-Ouchi (2004, 2010) with some changes; the domain of the 3-D model  
260 was the whole Antarctic continent, and the horizontal resolution was set to 32 km. The spatial  
261 distribution of the GHF was from Martos et al. (2017). The model was initialized using the present-  
262 day condition, and forced by the same temperature and SMB changes as those of the 1-D model forcing  
263 for the past 2 Ma (Fig. 3a). The migrations of the grounding lines were not forecasted, instead the  
264 positions of grounding lines were fixed to the present day. We note that the advancement of grounding  
265 lines during glacial periods has a minor impact on the ice thickness, in particular around the DF region,  
266 compared with the changes in climate forcing (Saito et al., 2010). We extracted the history of changes  
267 in the ice thickness at DF and EDC, which showed that the ice thickness was reduced by ~200 m during  
268 glacial periods, mainly because of reduced SMB (Fig. 3c).

269 Using this set of boundary conditions, we conducted simulations with different  $p$ -values (~~1-~~  
270 ~~5) and~~ GHFs (~~50-6070~~  $\text{mW m}^{-2}$ ) to calibrate the model with observed values at the DF ice core. We  
271 used the depth-age profile of the DF ice core, which was constructed by orbital tuning of a gas record  
272 above ~2500 m, and by matching to the AICC2012 chronology below that depth (Kawamura et al.,  
273 2017). We also used the measured depth-temperature profiles from the JARE54 surveys conducted  
274 during the 2012–2013 Antarctic summer (Buizert et al., 2021). The model was initialized with the  
275 conditions of 2 Ma BP, where the initial age and temperature were set to 0 years and  $-10\text{ }^{\circ}\text{C}$ ,  
276 respectively, for the entire ice column, respectively. All experiments were integrated for 2 Ma to reach  
277 the present day; therefore, the age of any ice older than 2 Ma did not appear in the experiments. These  
278 simplified initial conditions generated unrealistic temperature fields in the early stage of the simulation,  
279 but realistic glacial cycle forcing prevailed over the entire ice column within approximately 100 ka.  
280 Therefore, we mainly analyzed the results of the last 1.5 Ma, which is sufficient to discuss old ice in  
281 this study. Furthermore, we also applied this model to the conditions at EDC to check whether the  
282 model could simulate the observed temperature and age profiles at this location (Table 1).

283 We also conducted three sensitivity experiments to investigate the impacts of the  $p$  parameters,  
284 uncertainty in the amplitude of past temperature changes, and inclusion of past ice thickness changes,  
285 respectively. We found that  $p = 3$  gave one good age profile when compared with the ice-core data;  
286 hence, we set  $p = 3$  as the reference in Sect. 3. The uncertainty in the past temperature change was  
287 based on a study that proposed that the temperature change at the LGM in interior regions of the East  
288 Antarctic ice sheet was less than previously estimated (Buizert et al., 2021). We conducted a set of  
289 experiments where SAT anomalies were set to 0%, 25%, 50%, and 75% of the standard experiments,  
290 while keeping changes in SMB the same.

Parameters	DF	EDC
Ice thickness [m]	3028	3233
Surface mass <b>balance</b> [ice equivalent mm a <sup>-1</sup> ]	30.0	28.4
Surface temperature [°C]	-55.5	-54.65

292 **Table 1:** List of parameters used in Sect. 3. Ice thickness (DF and EDC), surface mass **balance**, and  
 293 surface temperature at EDC come from Parrenin et al. (2007); surface mass **balance** at DF comes from  
 294 Kameda et al. (2008) and Fujita et al. (2011); surface temperature at DF is calibrated in this study  
 295 ~~but~~ **and** is within previously observed ranges (Kameda et al., 1997; Yamanouchi et al., 2003).

296

297

### 3.2. Results for DF

298

299

300

301

302

303

304

305

306

307

308

309

310

311

312

313

314

315

316

317

318

319

320

321

322

323

324

325

326

327

328

329

330

331

332

333

334

335

336

In Fig. 4, the simulated temperature profiles at 0 ka (end of the simulations) with different GHFs under the same  $p$ -value ( $p = 3$ ) are compared with observations (Fig. 4a). The close-up of the bottom 120 m of the ice column is shown in Fig. 4b; the basal temperature ~~is was~~ well below melting point with a GHF of ~~5254 and 56~~ mW m<sup>-2</sup>, and at the melting point with a GHF > ~~5658~~ mW m<sup>-2</sup>. Compared with the observed temperature profile (Fig. 4, black lines), the simulated temperature near the ice base was colder by approximately 1 °C. In all simulations, the simulated temperature profiles were generally colder than observed temperature profiles ~~especially in the middle of the ice columns (Fig. 4a).~~ ~~especially in the middle of the ice columns (Fig. 4a).~~ ~~The generally colder temperature of the ice may have several explanations. One is related to the pressure melting point of the ice. We used a pressure melting point of ice that depended only on local pressure, but there is also a dependence on the impurities and air content of the ice (e.g., Parrenin et al., 2017; Passalacqua et al., 2017). A second explanation is related to the uncertainty in vertical velocity of the ice parameterized with  $p$  because a larger vertical advection contributes to a colder ice temperature.~~

The time series of simulated basal ice melting rates over the last 500 ka show that there have been significant temporal changes in these rates over time (Fig. ~~55a~~). With a GHF of ~~5254~~ mW m<sup>-2</sup>, the temperature at the ice base has been below the melting point through the last 500 ka. In contrast, in the case of a GHF of ~~5556~~ mW m<sup>-2</sup>, the basal melting rate is zero at 0 ka, while the maximum basal melting rate of 1 mm a<sup>-1</sup> occurs at the ~~end later stages~~ of interglacial periods (e.g., 100 ka BP). This ~~variability temporal variation~~ in basal melting rate is caused by glacial–cycle forcing in SAT and SMB, and minimum basal melting tends to occur ~~in at the interglacial end of glacial periods as it lags SAT.~~ This result is broadly consistent with previous studies (Saito and Abe-Ouchi, 2004; Van Liefferinge et al., 2018); ~~in that colder ice, which accumulated during glacial maximums, increased advection advects towards the ice base owing to an increased SMB during interglacials. A larger GHFs (<del>58 or</del> GHF ( $\geq 60$  mW m<sup>-2</sup>) results in basal melting occurring most of the time, with a an increase in basal melting rate of approximately 31 mm a<sup>-1</sup>. A downward flow of ice caused by basal melting (as in Equation 2) compensates for the basal melting owing to the increased downward advection every 5 mW m<sup>-2</sup> increase in GHF.~~

The simulated age profiles at the present day are compared with the ~~reconstructed ice core-based~~ profiles in Fig. 6a. With a small GHF (~~5254~~ mW m<sup>-2</sup>) where basal melting does not occur, the ice age at the ice–bedrock interface is > 1.5 Ma. In contrast, if basal melting occurs, the ice age at the ice–bedrock interface can be much younger; for example, ~~it is 980761 or 650620~~ ka for a GHF of ~~5560~~ or ~~5662~~ mW m<sup>-2</sup>, respectively. The result obtained with a GHF of ~~5560~~ mW m<sup>-2</sup> exhibits the closest fit to the data ~~at least 250 m above in terms of the bedrock. A larger GHF tends to decrease age of ice at the ice age, owing to a higher basal melting rate base of the ice column.~~ In this article, we define the “resolution of age” (ka m<sup>-1</sup>) as the inverse of annual layer thickness as an indicator of ~~old sufficient resolution for the chemical and isotopic contents of the~~ ice (Lilien et al., 2021). In Fig. 6b, the resolution of old ice is compared with the actual DF ice core. The model results largely reproduced the glacial–interglacial contrasts in annual layer thickness caused by the temporal variations of SMB at ~~the site this locality.~~ The observed resolution of age ~~is was~~ approximately 0.5–1 ka m<sup>-1</sup> near the base

337 of the ice core, and the model results using a GHF of 5560 mW m<sup>-2</sup> reproduced similar values.  
338 Furthermore, on the basis of Fig. 6b in a scenario with no significant basal melting, the annual layer  
339 thickness of 1.5 Ma BP ice is approximately 0.1 mm if the ice base temperature is well below the  
340 melting point (because 1.5 Ma ice appears directly above the bedrock (Fig. 6b, dark blue lines).

341 In accordance with the results described above, a larger GHF tends to result in a higher basal  
342 melting rate and younger age of ice at the base of the column. One critical point is that an excessive  
343 GHF (i.e., an increase of the order of 2 mW m<sup>-2</sup>) can have a considerable effect on the age of the ice  
344 and the likelihood of old ice. Next, we evaluate the effects of different vertical velocity profiles. In  
345 Figs 7 and 8, results with GHF of 55 mW m<sup>-2</sup> and different  $p$  values are compared. Generally, a larger  
346  $p$  value induces a colder temperature (Fig. 7a) and a lower basal melting rate (Fig. 7b). The simulated  
347 age profiles indicate that a larger  $p$  value induces a younger age of ice in the mid depths of the ice  
348 column (Fig. 8). Both of these results can be explained by differences in advection, in that a larger  $p$ -  
349 value induces larger advection of the temperature and age. Near the ice surface, the influence of basal  
350 melting is relatively small; therefore, a larger vertical velocity tends to result in a younger ice age. In  
351 contrast, near the base, a larger  $p$  value results in a colder basal temperature owing to greater advection  
352 of cold ice, which leads to less basal melting and an older ice age.

### 3.3. Results for EDC

353  
354 We also applied this model ~~to using~~ the EDC conditions at EDC to enable performance checks  
355 with one different at an additional location. We used the parameters listed in Table 21 and conducted  
356 sensitivity experiments with different GHFs. For the vertical velocity profile, we used  $p = 2.3$  following  
357 Parrenin et al. (2007). The model generally ~~results resulted~~ in colder temperatures compared with  
358 observations, similar to that found at DF (Fig. 9). The results7). We note that the pressure melting  
359 point of the ice depended only on local pressure in Fig. 7, but several studies have considered the  
360 pressure melting point of the ice as a function of the pressure and air content of the ice, which has  
361 shown that the basal temperature is at the pressure melting point (Buizert et al., 2021). Modeling using  
362 a GHF of 5456 mW m<sup>-2</sup> ~~gave gave~~ a basal ice age of approximately 900800 ka (Fig. 10a8a), which is  
363 ~~close similar~~ to the value (802 ka) presented in Veres et al. (2013), and the resolution of age closely fits  
364 the chronology estimated from ice-core analysis (Fig. 10b8b). One important result is that the threshold  
365 of GHF that allows basal melting is 54 mW m<sup>-2</sup> lower at EDC than at DF. This result is generally  
366 consistent compared with previous studies (Parrenin et al., 2007; Van Liefferinge et al., 2018). DF.  
367 This lower threshold of GHF can be attributed to the combination of larger ice thickness, smaller SMB,  
368 and higher SAT at the present day. The estimated GHF at EDC is smaller than that given by Parrenin  
369 et al. (2017), who estimated it to be 60 mW m<sup>-2</sup>. This difference can be attributed to the difference in  
370 the history of basal melting, or the application of past climate history derived from DF to EDC. The  
371 results from the application to EDC show that of our model produces results which are consistent with  
372 observations for slightly to EDC suggest that it may be applicable to different glaciological  
373 parameters conditions, particularly different ice thicknesses and SMBs.

### 3.4. Sensitivity of to vertical velocity profiles, temperature amplitudes, and ice thickness changes

374  
375  
376 Next, we evaluated the sensitivity of the temperature and age profiles to different vertical  
377 velocity profiles, temperature amplitudes, and ice thickness changes over glacial cycles. In Fig. 9,  
378 results using different  $p$  values under an identical GHF (60 mW m<sup>-2</sup>) are compared. A larger  $p$  value  
379 induced a lower basal melting rate because of a larger vertical velocity and downward advection of  
380 cold ice from the surface, although this only had a minor impact on the temperature profile. The  
381 simulated age profiles indicate that a larger  $p$  value induces a younger age of ice at mid-depths within  
382 the ice column (Fig. 9b), which is also a result of a larger vertical velocity. The age of the ice at the  
383 base of the column was approximately 800 ka BP in all five of the variable  $p$  value simulations, partly  
384 because of the compensating effects of greater advection and less basal melting.

385 The results using DF conditions with different ~~amplitude amplitudes~~ of temperature



387 ~~changes change~~ but ~~the same constant~~ GHF and  $p$  parameters (~~same as Sect.~~ GHF = 60 mW m<sup>-2</sup> and  $p$   
388  $\equiv 3.2$ ) are summarized in Fig. 11, ~~in terms of temperature and basal melting rates.~~ The control ~~10~~. Here,  
389 ~~we changed the  $\alpha$ -value in Equation 10 (1 is the control case).~~ In the smallest amplitude experiment ( $\alpha$   
390  $\equiv 0$ ), the temperature was set to the interglacial level and did not change in time. Note that the SMB  
391 ~~variation was the same in all sensitivity experiments exhibit.~~ The control experiments exhibited colder  
392 ice temperatures near the middle of the ice column ~~than compared with~~ observations, and this cold bias  
393 ~~can be was~~ reduced ~~if when~~ a smaller temperature amplitude over the glacial cycles ~~is was~~ used (Fig.  
394 ~~11a, 10a~~), broadly consistent with Buizert et al. (2021). ~~Temperature amplitude also changes basal~~  
395 ~~melting rates; a~~ smaller amplitude of the glacial cycle ~~contributes to~~ resulted in a younger age of ice  
396 ~~at the bottom of the ice column (Fig. 10b) because of~~ larger basal melting rates (Fig. ~~11b~~), 10c). This  
397 ~~is~~ because ~~the~~ mean temperature over the glacial cycles increases if ~~we reduce a smaller the~~ temperature  
398 amplitude of glacial–interglacial cycles ~~is reduced~~. The results using a fixed surface temperature ( $dT_s$   
399  $= 0.0$ ) ~~corresponded~~ corresponded to the same present-day SAT for the last 2 Ma, which ~~induces~~ induced  
400 basal melting of  $\sim 31.5$  mm a<sup>-1</sup> ~~during~~ most of ~~the this~~ time. A slight fluctuation in basal melting still  
401 ~~occurs~~ occurred owing to time-dependent SMB. ~~It is possible to tune the GHF as in Sect. 3.2, assuming~~  
402 ~~different temperature changes over the~~

403 ~~The results without ice thickness changes did not impact temperature profiles at the present-~~  
404 ~~day (Fig. 11a), but impacted the history of basal melting (Fig. 11c). The mean basal melting rates at~~  
405 ~~constant GHF can be reduced if ice thickness changes are included because the reduced ice thickness~~  
406 ~~during glacial periods decreases the pressure-melting point. Moreover, the inclusion of ice thickness~~  
407 ~~changes affects the phase of basal melting rates because it reflects the reduction in ice thickness and~~  
408 ~~pressure-melting point at the base of the ice during glacials. The minimum in basal melting during the~~  
409 ~~last glacial cycle. We regard this as an uncertainty in the forcing, and we note that it can change - occurs~~  
410 ~~at the end of the LGM in the control experiment; in contrast, it occurs at the present-day in the no ice~~  
411 ~~thickness change scenario. The absence of ice thickness changes results in larger mean~~ basal melting  
412 rates and a younger age of ice at the base of the ice column (Fig. 11b). These results suggest that the  
413 ~~basal melting rate in the past can be larger than the present-day rate.~~

### 415 3.5. Summary of Sect. 3

416 On the basis of the results described in this section, we conclude that using a combination of  $p$   
417  $= 3$  and GHF = ~~5560~~ mW m<sup>-2</sup> gives reasonable temperature and age profiles; ~~therefore.~~ Therefore, we  
418 decided to use these values as calibrated parameters for the DF region. ~~We use these parameters as a~~  
419 ~~calibrated values for the DF region; this was performed~~ for the following reasons. Later in the article,  
420 we investigate the possibility of old ice in the DF region using different parameters (~~i.e., spatially~~  
421 ~~variable of~~ ice thickness and GHF). ~~because glaciological surveys have suggested that there are spatial~~  
422 ~~variations in these parameters (e.g., Carson et al., 2013).~~ Hence, obtaining precise tuning at one specific  
423 DF location is unnecessary. ~~We~~ In this study, we calibrated the GHF under a vertical velocity profile  
424 ~~of  $p = 3$ , but calibrating the model with the combination of an uncertain GHF and vertical velocity~~  
425 ~~profile is possible. According to the age profile, the results with  $p = 3$  may not necessarily be the best~~  
426 ~~because the simulated age profile tends to underestimate the age of ice, particularly 500 m above the~~  
427 ~~bedrock. Therefore, we~~ do not state that ~~the a~~ GHF of ~~5560~~ mW m<sup>-2</sup> is a single best estimate for the  
428 DF location compared ~~to the with~~ previous estimates (Burton-Johnson et al., 2020; Talalay et al.,  
429 2021); ~~because there were assumptions made in the vertical velocity profiles and experimental design~~  
430 ~~of this study. Also~~ Furthermore, the calibrated GHF ~~depends~~ has some dependence on ~~chosen SAT~~  
431 ~~scenario~~ the uncertainty in temperature and ice thickness changes over the glacial cycles.

## 433 4. Sensitivity studies using various parameters around DF

### 434 4.1. Experimental design

435 This section investigates the impact of the ~~other~~ three parameters, ice thickness, SMB, and  
436 GHF, which may have spatial variations in the DF region. We investigated a range of ice thicknesses

between 2000 and 3200 m, based on an ice thickness map of the area around DF (Fig. 1). We used a present-day SMB range of 25–35 ice equivalent mm a<sup>-1</sup>. There is large uncertainty in GHF; we adopted a range of 50–70 mW m<sup>-2</sup>. The list of experiments is given in Table 2. Other aspects of the experimental design are the same as in Sect. 3.

Variable	Parameter range
Ice thickness [m]	2000–3200, every 100
Present-day SMB [ice equivalent mm a <sup>-1</sup> ]	25–35, every 1
GHF [mW m <sup>-2</sup> ]	50–70, every 2

Table 2: List of experiments in Sect. 4.

## 4.2. Results

In Fig. 12a, the relative effects of ice thickness and GHF on basal temperature are compared, using the same constant SMB (30 mm a<sup>-1</sup>). As in Sect. 3, we used an ice thickness of 3028 m, which is comparable to that at DF, and a threshold of GHF for basal melting of 5560 mW m<sup>-2</sup>. On the basis of the gradient of contours in Fig. 12a, an increase in ice thickness by 100 m has a comparable impact on the basal temperature as does an increase in GHF by 2 mW m<sup>-2</sup>. In Fig. 12b, the relative effects of ice thickness and SMB are compared using the same constant GHF (5560 mW m<sup>-2</sup>). A larger SMB results in a colder temperature; a 10% change in GHF leads to a ~4 °C change in the basal temperature, while a 10% change in SMB leads to a ~1 °C change. These results are generally consistent with those by Fischer et al. (2013). We note, and suggest that the spatial distribution of SMB (~20% for the DF area) has a minor impact on the basal temperature compared with that of the ice thickness.

— We further investigated the impact of different ice thicknesses on age profiles using the climatic conditions at DF (SMB = 30 ice equivalent mm a<sup>-1</sup>) and a calibrated GHF (5560 mW m<sup>-2</sup>). Figure 13a shows the simulated age of the ice at 50 and 100 m above the ice–bedrock interface, which were used as indicator depths for potential coring sites by Fischer et al. (2013). The results indicate that the rate of aging of ice rapidly decreases with ice thickness between 2800 and 3200 m owing to the occurrence of basal melting. Note that the age of 2 Ma BP is the limit of the experiments, and the results indicate that the old ice exists 50 m above the bedrock if the ice thickness is thicker than ~2100 m. Figure 13b shows the age resolution of the 1.5 Ma BP ice, indicating that a larger ice thickness tends to show a finer age resolution. The vertical age profiles and resolution of ice ages at three selected ice thicknesses (2200, 2600, and 3000 m) with the same constant GHF are shown in Fig. 14. According to Figure 14b, the expected age resolution of 1.5 Ma ice is approximately 10–ka m<sup>-1</sup> with an ice thickness of 2800 m, and 20 ka m<sup>-1</sup> with a smaller ice thickness of 2200 m.

## 5. Application to the DF–NDF transects

### 5.1. Experimental design

In this section, we apply the 1-D model to interpret the internal layers of the ice near DF, the structure of which was under idealized boundary conditions. Here, we used the dataset from 17<sup>th</sup> December, 2017 obtained by ground surveys during JARE59 (2017–2018). Here, we use the dataset from 17<sup>th</sup> December, 2017, which comprises a 54 km-long transect from DF to NDF (Fig. 1). The horizontal axis of Fig. 15 indicates the distance from DF, and the vertical axis indicates the depth from the surface. The gray shading indicates the reflectivity, which is an indicator of contours representing ice of the same age. The bedrock elevation, shown by brown lines, was detected based on the maximum reflectivity from the base (Tsutaki et al., 2022). The bedrock elevation was calibrated to match the observed bedrock elevation at DF. We calculated the 1-D age and temperature profiles of the ice at approximately 400 m intervals along the transect. We assumed that the vertical profile of vertical velocity could be determined locally using Equation 1, and that there were no horizontal interactions in temperature and age in this simulation. The present-day SMB was linearly interpolated between DF

483 (30 ice equivalent  $\text{mm a}^{-1}$ ) and NDF (25.5 ice equivalent  $\text{mm a}^{-1}$ ). ~~As there was~~ Note that the estimated  
484 SMB at NDF is 13% smaller than that at DF based on shallow ice cores (Oyabu et al., 2023). Because  
485 only very limited information ~~regarding~~ on the spatial distribution of GHF is available, we set a uniform  
486 value of 5560  $\text{mW m}^{-2}$  following the discussion in Sect. 3. As described in Sect. 3, the initial age of  
487 the ice was set to 0, the temperature set to  $-10\text{ }^{\circ}\text{C}$ , and the model was integrated over the last 2 Ma of  
488 forcing until it reached the present day (Fig. 3).

## 489 5.2. Results

491 In Fig. 15, the computed vertical profiles of the age are overlaid on a radargram using seven  
492 selected ages (colored lines), and the simulated basal temperature is indicated by shading in the bottom  
493 panel. The colored bar below the radargram indicates the simulated present-day basal temperature. The  
494 simulated distribution of ice age captured large-scale features in the black–white contour lines derived  
495 from the radargram signal (grayscale color in Fig. 15). The simulated age contours of 21 ka BP  
496 (approximately 500 m depth) and 128 ka BP (approximately 1500 m depth) can be traced from DF,  
497 although the deepest layer corresponding to an age older than 300 ka BP is hard to see in this image.  
498 Where ice is relatively thick (e.g., 20–25 km from DF), the simulated age of the ice at the ice–bedrock  
499 interface is younger than 700 ka BP, while ice older than 1.5 Ma BP occurs where the ice is relatively  
500 thin. On the basis of the results shown in Fig. 13b, we note that thin ice gives a poorer age resolution  
501 for the old ice. A comparison of the simulated ice age and ~~the~~ radargram signal gives an opportunity  
502 to examine the validity of the model results. For example, between 5 and 35 km from DF, the computed  
503 128 ka BP contour deviates to shallower levels (by 150 m from) compared with the tracked layer for  
504 the age obtained from the radar measurements, suggesting that the model overestimates the age of the  
505 ice near the bedrock in such locations.

## 506 6. Discussion

508 In this study, we used a 1-D ice-flow model, which computes the temporal evolution of age  
509 and temperature profiles. We used glaciological conditions at DF to tune some unknown parameters  
510 according to the observed temperature and age profiles. The results showed that the age profile is  
511 sensitive to the choice of GHF, but one experiment using a specific combination of GHF and vertical  
512 velocity profile exhibited reasonable temperature and age profiles (Figs 4 and 6). One important result  
513 is that the melting rate at the base of the ice exhibits temporal changes associated with glacial–  
514 interglacial forcing. This is caused by relatively cold ice deposited during glacial periods being pushed  
515 towards the bottom of the ice column by increased SMB and downward advection during interglacial  
516 periods, as shown in previous studies (e.g., Van Liefferinge et al., 2018). This point is critical for  
517 preserving old ice, ~~in that the temperature should be well below the melting point of the ice at the~~  
518 ~~present day~~ because basal melting rates during glacial periods past interglacials can be much higher  
519 than that of the present day (Fig. 5, ~~blue lines~~). Our sensitivity experiments highlighted the relative  
520 effects of ice thickness and GHF, whereby a small GHF excess above the condition that induces basal  
521 melting can result in a considerable reduction in the age of ice at the ice–bedrock interface (Fig. 6a).  
522 Below, we discuss the ~~limitation~~ limitations of the interpretations of our results, their relevance to  
523 previous ice-flow modeling studies, and uncertainty factors.

524 On the basis of data presented in Fig. 6, ~~the~~ a GHF of 5560  $\text{mW m}^{-2}$  sufficiently explains the  
525 observed temperature and age–depth profiles of the DF ice core. However, there is considerable  
526 uncertainty in the estimation of the actual GHF value at DF because of some simplifications in the  
527 model experiments and limited representations in physics. One point of difference is that the model  
528 tends to give a generally colder temperature profile compared with the observations (Fig. 4), which  
529 suggests that the model overestimates the GHF threshold of basal freezing. One possible reason for  
530 this difference is that the basal melting of ice can occur within a certain ice thickness; the extrapolation  
531 of observed temperature profiles at DF and EDC (Figs 4 and 97, black lines) shows that the ice reaches  
532 the pressure-melting point approximately 30 m above the bedrock. This feature cannot be simulated in

533 the model of the present study, which assumes that basal melting can only occur at the ice–bedrock  
534 interface. These representations in the physics of basal melting can be improved by using enthalpy as  
535 a state variable and adopting polythermal ice sheet models (e.g., Aschwanden et al., 2012). There is  
536 also uncertainty in the parameterization of the conductivity and heat capacity of the ice. We use these  
537 parameters as a function of temperature, but they can depend on the fabric of the ice, which makes it  
538 challenging to estimate them. Hence, these physical parameters can be a source of uncertainty in  
539 estimating GHF, and can be a source of difference from other studies. Another important factor in the  
540 temperature profiles is the temperature anomaly over glacial cycles, as a smaller glacial–interglacial  
541 temperature change tends to result in a warmer, more linear temperature profile compared with the  
542 control experiment (Fig. 4a10a). The temperature change over the last glacial cycle used in this study  
543 is based on deuterium and oxygen isotopes (Uemura et al., 2018), which exhibit an LGM temperature  
544 anomaly of approximately 8 °C (Fig. 3a). A recent study proposed that the temperature anomaly at the  
545 LGM at DF and EDC was about approximately half of the previous estimates based on the observed  
546 temperature profiles and other independent methods (Buizert et al., 2021). This study is in agreement  
547 with Buizert et al. (2021) in that our control experiment exhibits colder ice temperatures, especially at  
548 mid-depth within the ice column, and a smaller temperature difference between glacial and interglacial  
549 periods improves the modeled temperature profiles (Fig. 4a10a). If this is indeed the case, the actual  
550 threshold of the GHF value for the basal freezing should be lower than that used in the control  
551 experiment. We also found that if the temperature anomaly is half that of the control case, a GHF  
552 smaller than the control value (58 mW m<sup>-2</sup>) gives the closest age profile. We investigated the  
553 sensitivity to ice thickness as in Fig. 13, and obtained comparable results in terms of the age near the  
554 bottom of the ice column (not shown). These results indicate that several uncertainties (e.g., climate  
555 forcing and vertical velocity) can affect the temperature and age profiles under a certain condition, but  
556 if we calibrate the GHF with the DF ice-core age profile as in Sect. 3, we obtain comparable results  
557 regarding the sensitivity to ice thickness.

558 We note that the simulated age of the ice depends on the shape of the vertical velocity profile  
559 of the ice. The formulation of the present study has uses a smaller vertical ice velocity of the ice,  
560 especially near the base, compared with that used in Fischer et al. (2013). Because the age of the ice is  
561 related to the inverse of the vertical velocity, a different vertical velocity profile or a-p parameter can  
562 lead to a quantitatively different result. Moreover, vertical velocity profiles represented by a single *p*-  
563 value are merely one assumption; this formulation is derived from a solution of an idealized ice-sheet  
564 configuration (Liboutry, 1979), which may not be the case for realistic ice-sheet sheets. For example,  
565 the observed magnitude of layer thinning of the DF ice core exhibits a decreasing trend over the bottom  
566 500 m (Fig. 6). According to analyses of the DF ice core (Azuma et al., 1999; Saruya et al., 2022) or  
567 3-D ice sheet modeling (Seddik et al., 2011), deformation of the ice or flow regime towards the ice  
568 bottom of the ice is complex. Thus, we suggest that both horizontal and vertical ice flow should be  
569 complex as well, which may be difficult to represent by using the current formulation of vertical  
570 velocity profiles.

571 We also note that the resolution of 1.5 Ma ice, one indicator of old ice, depends on ice thickness.  
572 In particular, Lilien et al. (2021) presented similar 1-D ice-flow model results from BELDC (Beyond  
573 EPICA Little Dome C, ice thickness of ~2750 m) constrained by radar-imaged internal layers and  
574 estimated the resolution of 1.5 Ma ice as  $19 \pm 2 \text{ ka m}^{-1}$ . In contrast, our results for EDC conditions  
575 have a resolution of the ice (with a small enough GHF to keep the base of the ice frozen) have an ice  
576 age resolution of approximately  $10 \text{ ka m}^{-1}$  (Fig. 408, dark blue lines), which is approximately half of  
577 that in Lilien et al. (2021). This difference can be attributed to the combination of the model  
578 parameters, such as ice thickness, *p* of the vertical velocity profile, or SMB history (3233 m and *p* =  
579 2.3 in this study), because the two studies adopted the same formulation of the vertical velocity profile.  
580 According to Figs 13 and 14, a larger ice thickness leads to a better resolution of the ice age if the base  
581 of the ice is remains frozen throughout time. Therefore, we speculate that the different ice thickness, p-  
582 value, or SMB history (3233 m for EDC) would be the most critical factor in the Lilien et al. (2021)

583 ~~study (whose value ranges were not explicitly presented) may have caused the~~ difference in the age  
584 resolution of 1.5 Ma BP ~~ice~~ when compared with Lilien et al. (2021), who used BELDC conditions  
585 (ice thickness of 2750 m).

586 Application of the 1-D model to the transect between DF and NDF provides an opportunity to  
587 examine the influence of spatially varying glaciological conditions (e.g., ice thickness and GHF) on  
588 the age of the ice. The simulated age–depth distributions with constant GHF but different ice thickness  
589 and SMB exhibit general agreement with observed internal layers (Fig. 15). One noticeable model–  
590 data discrepancy occurs at 14–18 km from DF, where the simulated age contours of 128 ka BP are  
591 ~150 m above the observed internal layers traced from DF. This model–data discrepancy indicates that  
592 the effects of vertical or horizontal advection (Huybrechts et al., 2007; Sutter et al., 2021), or ~~ice~~  
593 ~~thickness changes over glacial cycles (Saito et al., 2020)~~ spatial distribution of GHF may have  
594 contributed to this difference. Although the relative importance of the spatial distributions of GHF,  
595 SMB, and horizontal flow is difficult to assess in the present study, we expect that future glaciological  
596 data constraints and model developments will better constrain these uncertain parameters and the  
597 spatial distribution of old ice. One recently published present-day SMB from the vicinity of the DF  
598 region exhibits spatial variabilities reflecting surface topographical features (Van Liefferinge et al.,  
599 2021). On the basis of systematic sensitivity experiments (Sect. 4), we have shown that the impact of  
600 SMB on the age of the ice is relatively minor compared with that of ice thickness, but the small-scale  
601 features present in internal layers of the ice can be improved by using the spatial distribution of present-  
602 day SMB, and this will contribute to the selection of the most suitable drilling site.

## 603 604 7. Conclusions

605 We draw the following conclusions from this study.

- 606 1. In experiments using the ~~configurations of DF configuration~~, the model largely reproduced the  
607 observed age and temperature profiles under a calibrated GHF. If the GHF is small enough to keep  
608 the basal temperature below the melting point, it is expected that ~1.5 Ma ice could be present. ~~If~~  
609 ~~such old ice exists~~ According to Figs 14 and 15, the simulated annual layer thickness of ~1.5 Ma  
610 BP ice is approximately ~0.05 to 0.1 mm, which corresponds to 10 to 20 ka m<sup>-1</sup>. According to  
611 IPICS, this is a feasible resolution for analysis with minimized effects of diffusion. This is also  
612 true for EDC, but the threshold of GHF for basal melting is different because of a different ice  
613 thickness and SMB.
- 614 2. Under the configuration and range of parameters of the present study, the ice thickness has a larger  
615 impact on basal melting than does the present-day SMB; an ice thickness difference of ~100 m  
616 corresponds to ~~an~~ SMB difference of 5 ice equivalent mm a<sup>-1</sup> (Fig. 12). Near the DF region, the  
617 ice thickness ~~has larger exceeds such a~~ spatial variability ~~above these ranges~~, while SMB does not.  
618 ~~Though~~ Although there is considerable uncertainty in the spatial distribution of GHF, ice thickness  
619 is suggested to be one of the most critical factors for the preservation of old ice.
- 620 3. ~~The climate forcing of the past influences the temperature and age profiles, and induces a~~  
621 ~~substantial change in basal melting rates. The calibrated age profile at DF resulted from temporally~~  
622 ~~evolving basal melting rates, which mostly occurred after interglacial periods. This temporally~~  
623 ~~changing basal melting can eliminate the old ice of ~1.5 Ma BP. The calibrated GHF in this study,~~  
624 ~~which is based on an ice-core age profile, has uncertainties. The basal melting rate, which is critical~~  
625 ~~to the age of ice near the bottom of the column, is determined by the thermal conditions. The basal~~  
626 ~~melting exhibits temporal variability as a result of glacial–interglacial changes in climate, and the~~  
627 ~~maximum basal melting tends to occur at the end of interglacials. Thus, the basal melting is~~  
628 ~~influenced by climate forcing of past temperature and ice thickness changes, which have~~  
629 ~~uncertainties. Furthermore, a vertical velocity profile parameterized with a uniform  $p$ -value can~~  
630 ~~be a source of uncertainty, and may have a limited ability to represent complex ice flow near the~~  
631 ~~bottom of the ice column.~~
- 632 4. From the simulation of the DF–NDF transect, a small ice thickness and colder basal temperature

633 are the necessary conditions for the presence of ~~the old ice of~~ (~1.5 Ma) ice. However, a small  
634 ice thickness contributes to a coarser resolution of the old ice (small annual layer thickness), which  
635 may make it difficult to extract paleoclimate information. As discussed in Pattyn (2010), ice  
636 thickness is found to be a compromising factor in the selection of a drilling site.

- 637 5. The simulation along the DF–NDF transect does not reproduce the depth of the internal layers of  
638 the ice corresponding to 128 ka BP at some locations (e.g., at distances 5–35 km from DF),  
639 suggesting a possible error in the simulated age of ice near the bottom of the ice column. The  
640 simulated age of ice in this area, especially where there is a large discrepancy between the  
641 simulation and radar images, could be caused by uncertainties derived from several assumptions  
642 or uncertainty in the model or methods, including spatial distributions of GHF, representation in  
643 vertical temperature profile that depends only on normalized altitude (DF ice core suggests  
644 complex ice-flow near its base), representation in thermodynamics associated with basal melting,  
645 or history of surface temperature changes. Therefore, future improvements in numerical models  
646 and methods would contribute to better constraining the age of the ice.

647 A recent compilation of ice thickness data around DF indicates the presence of complex and steep  
648 terrain in the area, with uncertainty in bedrock elevation of > 60 m (Tsutaki et al., 2022), highlighting  
649 the necessity of a high-spatial-resolution survey of bedrock topography. The results from this study  
650 help to support the interpretation of observational data and the selection of a suitable drilling site.

#### 651 **Code availability:**

652 The numerical model is available from Github. <https://github.com/saitofuyuki/icies2.git>  
653  
654

#### 655 **Data availability:**

656 The scripts and data for conducting experiments and analyzing results are available at AORI-CESD  
657 (<https://cesd.auri.u-tokyo.ac.jp/cesddb/publication/index.html>). All figures were generated using GMT  
658 version 4.5.9. The ice core chronology and temperature at DF are available from previously published  
659 articles (Veres et al., 2013; Kawamura et al., 2017; Buizert et al., 2021).  
660

#### 661 **Author contribution**

662 T. O., A. A-O., and F. S. conceived the study, developed the numerical model, designed and carried  
663 out the experiments, and analyzed the results. T. S., S. F., K. K., and H. M. provided glaciological data  
664 from JARE surveys and contributed to the experimental design. T. O. prepared the manuscript with  
665 contributions from all co-authors.  
666

#### 667 **Competing interests**

668 The authors declare that they have no conflict of interest.  
669

#### 670 **Acknowledgments**

671 We would like to thank Frédéric Parrenin and two anonymous referees for their valuable comments,  
672 which have substantially improved our manuscript. We thank Kenichi Matsuoka, Brice Van  
673 Liefferinge, and Ralf Greve for their fruitful discussions. This research was supported by JSPS  
674 Kakenhi JP17H06104, JP17H06323, and JP18H05294. T. O., A. A-O., and F. S. were supported by  
675 JPJSBP120213203. F. S. was also supported by JSPS Kakenhi JP17K05664. We thank David Wacey,  
676 PhD, from Edanz (<https://jp.edanz.com/ac>) for editing a draft of this manuscript.  
677

#### 678 **References**

- 679 1. Abe-Ouchi, A., Saito, F., Kawamura, K., Raymo, M. E., Okuno, J., Takahashi, K., and Blatter, H..  
680 Insolation-driven 100,000-year glacial cycles and hysteresis of ice-sheet volume. *Nature* 500,  
681 190–193, doi: 10.1038/nature12374, 2013

- 682 2. Aschwanden, A., Bueler, E., Khroulev, C., and Blatter, H.: An enthalpy formulation for glaciers  
683 and ice sheets, *J. Glaciol.*, 58, 441-457, doi:10.3189/2012JoG11J088, 2012.
- 684 3. Azuma, N., Wang, Y., Mori, K., Narita, H., Hondoh, T., Shoji, H., and Watanabe O.: Textures and  
685 fabrics in the Dome F (Antarctica) ice core, *Ann. Glaciol.*, 29, 163-168,  
686 <https://doi.org/10.3189/172756499781821148>, 1999.
- 687 4. Bracegirdle, T. J., Krinner, G., Tonelli, M., et al. Twenty first century changes in Antarctic and  
688 Southern Ocean surface climate in CMIP6. *Atmos Sci Lett.*, doi: 10.1002/asl.984, 2020
- 689 5. Burton-Johnson, A., Dziadek, R., and Martin, C., Geothermal heat flow in Antarctica: current and  
690 future directions, *The Cryosphere*, 14, 3843–3873, doi:10.5194/tc-14-3843-2020, 2020
- 691 6. Buizert, C., Fudge, T. J., Roberts, W. H., Steig, E. J., Sherriff-Tadano, S., Ritz, C., Lefebvre, E.,  
692 Edwards, J., Kawamura, K., Oyabu, I., and Motoyama, H. et al.: Antarctic surface temperature  
693 and elevation during the Last Glacial Maximum, *Science* 372(6546), 1097-1101, doi:  
694 10.1126/science.abd2897, 2021
- 695 7. Carson, C. J., McLaren, S., Roberts, J. L., Boger, S. D., and Blankenship, D. D.: Blankenship, hot  
696 rocks in a cold place: High sub-glacial heat flow in East Antarctica, *J. Geol. Soc. London*, 171, 9–  
697 12, <https://doi.org/10.1144/jgs2013-030>, 2014.
- 698 7-8. Clark, P., Archer, D., Pollard, D., Blum, J. D., Rial, J. A., Brovkin, V., Mix, A. C., Pisias, N. G.  
699 and Roy, M.: The middle Pleistocene transition: characteristics, mechanisms, and implications for  
700 long-term changes in atmospheric pCO<sub>2</sub>, *Quaternary Science Reviews*, 25, 23–24, 3150-3184.  
701 doi: 10.1016/j.quascirev.2006.07.008, 2006
- 702 8-9. Fischer, H., Severinghaus, J., Brook, E., Wolff, E., Albert, M., Alemany, O., Arthern, R., Bentley,  
703 C., Blankenship, D., Chappellaz, J., Creyts, T., Dahl-Jensen, D., Dinn, M., Frezzotti, M., Fujita,  
704 S., Gallee, H., Hindmarsh, R., Hudspeth, D., Jugie, G., Kawamura, K., Lipenkov, V., Miller, H.,  
705 Mulvaney, R., Parrenin, F., Pattyn, F., Ritz, C., Schwander, J., Steinhage, D., van Ommen, T., and  
706 Wilhelms, F.: Where to find 1.5 million yr old ice for the IPICS “Oldest-Ice” ice core, *Clim. Past*,  
707 9, 2489–2505, doi:10.5194/cp-9-2489-2013, 2013.
- 708 9-10. Fox-Kemper, B., H. T. Hewitt, C. Xiao, G. Adalgeirsdottir, S. S. Drijfhout, T. L. Edwards, N.  
709 R. Golledge, M. Hemer, R. E. Kopp, G. Krinner, A. Mix, D. Notz, S. Nowicki, I. S. Nurhati, L.  
710 Ruiz, J-B. Sallee, A. B. A. Slangen, Y. Yu: Ocean, Cryosphere and Sea Level Change. In: *Climate*  
711 *Change 2021: The Physical Science Basis. Contribution of Working Group I to the Sixth*  
712 *Assessment Report of the Intergovernmental Panel on Climate Change [Masson-Delmotte, V., P.*  
713 *Zhai, A. Pirani, S. L. Connors, C. Pean, S. Berger, N. Caud, Y. Chen, L. Goldfarb, M. I. Gomis,*  
714 *M. Huang, K. Leitzell, E. Lonnoy, J.B.R. Matthews, T. K. Maycock, T. Waterfield, O. Yelekci,*  
715 *R. Yu and B. Zhou (eds.)]. Cambridge University Press, 2021.*
- 716 10-11. Frieler, K., Clark, P., He, F. et al. Consistent evidence of increasing Antarctic accumulation  
717 with warming. *Nature Clim Change* 5, 348–352. doi: 10.1038/nclimate2574, 2015.
- 718 11-12. Fretwell, P., Pritchard, H. D., Vaughan, D. G., Bamber, J. L., Barrand, N. E., Bell, R., Bianchi,  
719 C., Bingham, R. G., Blankenship, D. D., Casassa, G., Catania, G., Callens, D., Conway, H., Cook,  
720 A. J., Corr, H. F. J., Damaske, D., Damm, V., Ferraccioli, F., Forsberg, R., Fujita, S., Gim, Y.,  
721 Gogineni, P., Griggs, J. A., Hindmarsh, R. C. A., Holmlund, P., Holt, J. W., Jacobel, R. W.,  
722 Jenkins, A., Jokat, W., Jordan, T., King, E. C., Kohler, J., Krabill, W., Riger-Kusk, M., Langlely,  
723 K. A., Leitchenkov, G., Leuschen, C., Luyendyk, B. P., Matsuoka, K., Mouginot, J., Nitsche, F.  
724 O., Nogi, Y., Nost, O. A., Popov, S. V., Rignot, E., Rippin, D. M., Rivera, A., Roberts, J., Ross,  
725 N., Siegert, M. J., Smith, A. M., Steinhage, D., Studinger, M., Sun, B., Tinto, B. K., Welch, B. C.,  
726 Wilson, D., Young, D. A., Xiangbin, C., and Zirizzotti, A.: Bedmap2: improved ice bed, surface  
727 and thickness datasets for Antarctica, *The Cryosphere*, 7, 375–393, doi: 10.5194/tc-7-375-2013,  
728 2013.
- 729 12-13. Fujita, S., Holmlund, P., Andersson, I., Brown, I., Enomoto, H., Fujii, Y., Fujita, K., Fukui, K.,  
730 Furukawa, T., Hansson, M., Hara, K., Hoshina, Y., Igarashi, M., Iizuka, Y., Imura, S., Ingvander,  
731 S., Karlin, T., Motoyama, H., Nakazawa, F., Oerter, H., Sjöberg, L. E., Sugiyama, S., Surdyk, S.,

- 732 Ström, J., Uemura, R., and Wilhelms, F.: Spatial and temporal variability of snow accumulation  
733 rate on the East Antarctic ice divide between Dome Fuji and EPICA DML, *The Cryosphere*, 5,  
734 1057–1081, doi:10.5194/tc-5-1057-2011, 2011.
- 735 ~~13~~14. Greve, R., and Blatter, H. K.: *Dynamics of Ice Sheets and Glaciers*, Springer, Berlin, 2009.
- 736 ~~14~~15. Hondoh, T., Shoji, H., Watanabe, O., Salamatin, A. N., and Lipenkov, V. Y.: Depth-age and  
737 temperature prediction at Dome Fuji station, East Antarctica, *Ann. Glaciol.*, 35, 384–390,  
738 <https://doi.org/10.3189/172756402781817013>, 2002.
- 739 ~~15~~16. Huybrechts, P. and Oerlemans, J.: Response of the Antarctic ice sheet to future greenhouse  
740 warming, *Climate Dynamics*, 5, 93–102, 1990.
- 741 ~~16~~17. Huybrechts, P., Rybak, O., Pattyn, F., Ruth, U., and Steinhage, D.: Ice thinning, upstream  
742 advection, and non-climatic biases for the upper 89% of the EDML ice core from a nested model  
743 of the Antarctic ice sheet, *Clim. Past*, 3, 577–589, <https://doi.org/10.5194/cp-3-577-2007>, 2007.
- 744 ~~17~~18. Jouzel, J., Masson-Delmotte, V., Cattani, O., Dreyfus, G., Falourd, S., Hoffmann, G., Minster,  
745 B., Nouet, J., Barnola, J. M., Chappellaz, J., Fischer, H., Gallet, J. C., Johnsen, S., Leuen-berger,  
746 M., Loulergue, L., Luethi, D., Oerter, H., Parrenin, F., Raisbeck, G., Raynaud, D., Schilt, A.,  
747 Schwander, J., Selmo, E., Souchez, R., Spahni, R., Stauffer, B., Steffensen, J. P., Stenni, B.,  
748 Stocker, T. F., Tison, J. L., Werner, M., and Wolff, E. W.: Orbital and Millennial Antarctic Climate  
749 Variability over the Past 800,000 Years, *Science*, 317, 793–796,  
750 <https://doi.org/10.1126/science.1141038>, 2007.
- 751 ~~18~~19. Kameda, T., Azuma, N., Furukawa, T., Ageta, Y. and Takahashi, S.: Surface mass balance,  
752 sublimation and snow temperatures at Dome Fuji Station, Antarctica, in 1995. *Proc. NIPR Symp.*  
753 *Polar Meteorol. Glaciol.*, 11, 24–34, 1997
- 754 ~~19~~20. Kameda, T., Motoyama, H., Fujita, S., and Takahashi, S.: Temporal and spatial variability of  
755 surface mass balance at Dome Fuji, East Antarctica, by the stake method from 1995 to 2006, *J.*  
756 *Glaciol.*, 54, 107–116, doi:10.3189/002214308784409062, 2008.
- 757 ~~20~~21. Karlsson, N. B., Binder, T., Eagles, G., Helm, V., Pattyn, F., Van Liefferinge, B., and Eisen,  
758 O.: Glaciological characteristics in the Dome Fuji region and new assessment for “Oldest Ice”,  
759 *The Cryosphere*, 12, 2413–2424, doi:10.5194/tc-12-2413-2018, 2018.
- 760 ~~21~~22. Kawamura, K., Parrenin, F., Uemura, R., Vimeux, F., Severinghaus, J. P., Hutterli, M. A.,  
761 Nakazawa, T., Aoki, S., Jouzel, J., Raymo, M. E., Matsumoto, K., Nakata, H., Motoyama, H.,  
762 Fujita, S., Goto-Azuma, K., Fujii, Y., and Watanabe, O.: Northern Hemisphere forcing of climatic  
763 cycles in Antarctica over the past 360,000 years *Nature*, 448, 912–917, doi:10.1038/nature06015,  
764 2007.
- 765 ~~22~~23. Kawamura, K., Abe-Ouchi, A., Motoyama, H., Ageta, Y., Aoki, S., Azuma, N., Fujii, Y.,  
766 Fujita, K., Fujita, S., Fukui, K., Furukawa, T., Furusaki, A., Goto-Azuma, K., Greve, R.,  
767 Hirabayashi, M., Hondoh, T., Hori, A., Horikawa, S., Horiuchi, K., Igarashi, M., Iizuka, Y.,  
768 Kameda, T., Kanda, H., Kohno, M., Kuramoto, T., Matsushi, Y., Miyahara, M., Miyake, T.,  
769 Miyamoto, A., Nagashima, Y., Nakayama, Y., Nakazawa, T., Nakazawa, F., Nishio, F., Obinata,  
770 I., Ohgaito, R., Oka, A., Okuno, J., Okuyama, J., Oyabu, I., Parrenin, F., Pattyn, F., Saito, F., Saito,  
771 T., Saito, T., Sakurai, T., Sasa, K., Seddik, H., Shibata, Y., Shinbori, K., Suzuki, K., Suzuki, T.,  
772 Takahashi, A., Takahashi, K., Takahashi, S., Takata, M., Tanaka, Y., Uemura, R., Watanabe, G.,  
773 Watanabe, O., Yamasaki, T., Yokoyama, K., Yoshimori, M., and Yoshimoto, T.: State dependence  
774 of climatic instability over the past 720,000 years from Antarctic ice cores and climate modeling,  
775 *Sci. Adv.*, 3, 1–13, doi:10.1126/sciadv.1600446, 2017.
- 776 ~~23~~24. Lilien, D. A., Steinhage, D., Taylor, D., Parrenin, F., Ritz, C., Mulvaney, R., Martín, C., Yan,  
777 J.-B., O'Neill, C., Frezzotti, M., Miller, H., Gogineni, P., Dahl-Jensen, D., and Eisen, O.: Brief  
778 communication: New radar constraints support presence of ice older than 1.5 Myr at Little Dome  
779 C, *The Cryosphere*, 15, 1881–1888, doi:10.5194/tc-15-1881-2021, 2021.
- 780 ~~24~~25. Lisiecki, L. E. and Raymo, M. E.: A Pliocene-Pleistocene stack of 57 globally distributed  
781 benthic  $\delta^{18}O$  records, *Paleoceanography*, 20, PA1003, doi:10.1029/2004PA001071, 2005



- 782 [25.26.](#) Lliboutry, L.: A critical review of analytical approximate solutions for steady state velocities  
783 and temperatures in cold ice-sheets, *Z. Gletscherkd. Glazialgeol.*, 15, 135–148, 1979
- 784 [27.](#) [Martos, Y. M., Catalan, M., Jordan, T. A., Golynsky, A., Golynsky, D., Eagles, G., and Vaughan,](#)  
785 [D. G.: Heat flux distribution of Antarctica unveiled, \*Geophys. Res. Lett.\*, 44, 11417–11426,](#)  
786 <https://doi.org/10.1002/2017GL075609>, 2017.
- 787 [26.28.](#) Motoyama H, Takahashi, A., Tanaka, Y., Shinbori, K., Miyahara, M., Yoshimoto, T., Fujii, Y.,  
788 Furusaki, A., Azuma, N., Ozawa, Y., Kobayashi, K., and Yoshise, Y. : Deep ice core drilling to a  
789 depth of 3035.22m at Dome Fuji, Antarctica in 2001–07. *Annals of Glaciology*, 62, 212–222,  
790 doi:10.1017/aog.2020.84, 2021
- 791 [27.29.](#) Mouginot, J., B. Scheuchl, and E. Rignot: Mapping of Ice Motion in Antarctica Using  
792 Synthetic-Aperture Radar Data, *Remote Sensing*. 4. 2753–2767. doi: 10.3390/rs4092753, 2012.
- 793 [28.30.](#) Obase, T., A. Abe-Ouchi, F. Saito: Abrupt climate changes in the last two deglaciations  
794 simulated with different Northern ice sheet discharge and insolation, *Scientific Reports*, 11, doi:  
795 10.1038/s41598-021-01651-2, 2021
- 796 [31.](#) [Oyabu, I., Kawamura, K., Fujita, S., Inoue, R., Motoyama, H., Fukui, K., Hirabayashi, M.,](#)  
797 [Hoshina, Y., Kurita, N., Nakazawa, F., Ohno, H., Sugiura, K., Suzuki, T., Tsutaki, S., Abe-Ouchi,](#)  
798 [A., Niwano, M., Parrenin, F., Saito, F., and Yoshimori, M.: Temporal variations of surface mass](#)  
799 [balance over the last 5000 years around Dome Fuji, Dronning Maud Land, East Antarctica, \*Clim.\*](#)  
800 [Past](#), 19, 293–321, <https://doi.org/10.5194/cp-19-293-2023>, 2023.
- 801 [29.32.](#) Paillard, D. Glacial cycles: Toward a new paradigm, *Review of Geophysics*, 39, 3,  
802 <https://doi.org/10.1029/2000RG000091>, 2001.
- 803 [30.33.](#) Pattyn, F.: Antarctic subglacial conditions inferred from a hybrid ice sheet/ice stream model,  
804 *Earth. Planet. Sci. Lett.*, 295, 451–461, doi:10.1016/j.epsl.2010.04.025, 2010.
- 805 [31.34.](#) Parrenin, F., Barnola, J.-M., Beer, J., Blunier, T., Castellano, E., Chappellaz, J., Dreyfus, G.,  
806 Fischer, H., Fujita, S., Jouzel, J., Kawamura, K., Lemieux-Dudon, B., Loulergue, L., Masson-  
807 Delmotte, V., Narcisi, B., Petit, J.-R., Raisbeck, G., Raynaud, D., Ruth, U., Schwander, J., Severi,  
808 M., Spahni, R., Steffensen, J. P., Svensson, A., Udisti, R., Waelbroeck, C., and Wolff, E.: The  
809 EDC3 chronology for the EPICA Dome C ice core, *Clim. Past*, 3, 485–497, doi:10.5194/cp-3-  
810 485-2007, 2007.
- 811 [35.](#) Parrenin, F., and Hindmarsh, R.: [Influence of a non-uniform velocity field on isochrone geometry](#)  
812 [along a steady flowline of an ice sheet, \*Journal of Glaciology\*, 53, 183, 612–622, doi:](#)  
813 [10.3189/002214307784409298](https://doi.org/10.3189/002214307784409298), 2007.
- 814 [32.36.](#) Parrenin, F., Fujita, S., Abe-Ouchi, A., Kawamura, K., Masson-Delmotte, V., Motoyama, H.,  
815 Saito, F., Severi, M., Stenni, B., Uemura, R., and Wolff, E.: Climate dependent contrast in surface  
816 mass balance in East Antarctica over the past 216 ka, *J. Glaciol.*, 36, 455–466,  
817 doi:10.1017/jog.2016.85, 2016.
- 818 [33.37.](#) Parrenin, F., Cavitte, M. G. P., Blankenship, D. D., Chappellaz, J., Fischer, H., Gagliardini, O.,  
819 Masson-Delmotte, V., Passalacqua, O., Ritz, C., Roberts, J., Siegert, M. J., and Young, D. A.: Is  
820 there 1.5-million-year-old ice near Dome C, Antarctica?, *The Cryosphere*, 11, 2427–2437, doi:  
821 10.5194/tc-11-2427-2017, 2017.
- 822 [34.38.](#) Passalacqua, O., Ritz, C., Parrenin, F., Urbini, S., and Frezzotti, M.: Geothermal flux and basal  
823 melt rate in the Dome C region inferred from radar reflectivity and heat modelling, *The*  
824 *Cryosphere*, 11, 2231–2246, <https://doi.org/10.5194/tc-11-2231-2017>, 2017.
- 825 [35.39.](#) Passalacqua, O., Cavitte, M., Gagliardini, O., Gillet-Chaulet, F., Parrenin, F., Ritz, C., and  
826 Young, D.: Brief communication: Candidate sites of 1.5 Myr old ice 37 km southwest of the Dome  
827 C summit, East Antarctica, *The Cryosphere*, 12, 2167–2174, doi:10.5194/tc-12-2167-2018, 2018.
- 828 [36.40.](#) Rignot, E., J. Mouginot, and B. Scheuchl: Ice Flow of the Antarctic Ice Sheet, *Science*. 333.  
829 1427–1430. doi: 10.1126/science.1208336, 2011.
- 830 [37.41.](#) Rignot, E., J. Mouginot, and B. Scheuchl: MEaSURES InSAR-Based Antarctica Ice Velocity  
831 Map, Version 2. Boulder, Colorado USA. NASA National Snow and Ice Data Center Distributed

832 Active Archive Center. doi: 10.5067/D7GK8F5J8M8R, 2017.

833 ~~38-42.~~ Ritz, C.: Time dependent boundary conditions for calculation of temperature fields in ice  
834 sheets. In: E. D. Waddington and J. S. Walder (Eds.), *The Physical Basis of Ice Sheet Modelling*,  
835 IAHS Publication No. 170, pp. 207-216. IAHS Press, Wallingford, UK, 1987.

836 ~~39-43.~~ Rodrigez-Morales, F. Braaten, D., Mai, H. T., Paden, J., Gogineni, P., Yan, J-B., Abe-Ouchi,  
837 A., Fujita, S., Kawamura, K., Tsutaki, S., Van Liefferinge, B., Matsuoka, K., and Steinhage, D.:  
838 A Mobile, Multi-Channel, UWB Radar for Potential Ice Core Drill Site Identification in East  
839 Antarctica: Development and First Results, *IEEE Journal of Selected Topics in Applied Earth  
840 Observations and Remote Sensing*, 13, 4836-4847, 2020.

841 ~~40-44.~~ Saito, F. and A. Abe-Ouchi.: Thermal structure of Dome Fuji and east Dronning Maud Land,  
842 Antarctica, simulated by a three-dimensional ice-sheet model, *Ann. Glaciol.*, 39, 433–438, doi:  
843 10.3189/172756404781814258, 2004.

844 ~~41-45.~~ Saito, F., and Abe-Ouchi, A.: Modelled response of the volume and thickness of the Antarctic  
845 ice sheet to the advance of the grounded area, *Ann. of Glaciol.*, 51, 41-48, doi:  
846 10.3189/172756410791392808, 2010.

847 ~~42-46.~~ Saito, F., Obase, T., and Abe-Ouchi, A.: Implementation of the RCIP scheme and its  
848 performance for 1-D age computations in ice-sheet models, *Geosci. Model Dev.*, 13, 5875–5896,  
849 doi:10.5194/gmd-13-5875-2020, 2020.

850 ~~43-47.~~ Saruya, T., Fujita, S., Iizuka, Y., Miyamoto, A., Ohno, H., Hori, A., Shigeyama, W.,  
851 Hirabayashi, M., and Goto-Azuma, K.: Development of crystal orientation fabric in the Dome Fuji  
852 ice core in East Antarctica: implications for the deformation regime in ice sheets, *The Cryosphere*,  
853 16, 2985–3003, <https://doi.org/10.5194/tc-16-2985-2022>, 2022.

854 ~~44-48.~~ Seddik, H., Greve, R., Zwinger, T., and Placidi, L.: A full Stokes ice flow model for the vicinity  
855 of Dome Fuji, Antarctica, with induced anisotropy and fabric evolution, *The Cryosphere*, 5, 495–  
856 508, doi:10.5194/tc-5-495-2011, 2011.

857 ~~49.~~ [Shakun, J. D., Lea, D. W., Lisiecki, L. E., and Raymo, M. E.: An 800-kyr record of global surface  
858 ocean delta O-18 and implications for ice volume-temperature coupling, \*Earth Planet. Sc. Lett.\*,  
859 \*426\*, 58-68, doi:10.1016/j.epsl.2015.05.042](#)

860 ~~45-50.~~ Sun, B., Moore, J. C., Zwinger, T., Zhao, L., Steinhage, D., Tang, X., Zhang, D., Cui, X., and  
861 Martín, C.: How old is the ice beneath Dome A, Antarctica?, *The Cryosphere*, 8, 1121–1128,  
862 doi:10.5194/tc-8-1121-2014, 2014.

863 ~~46-51.~~ Sutter, J., Fischer, H., Grosfeld, K., Karlsson, N. B., Kleiner, T., Van Liefferinge, B., and Eisen,  
864 O.: Modelling the Antarctic Ice Sheet across the mid-Pleistocene transition – implications for  
865 Oldest Ice, *The Cryosphere*, 13, 2023–2041, <https://doi.org/10.5194/tc-13-2023-2019>, 2019.

866 ~~47-52.~~ Sutter, J., Fischer, H., and Eisen, O.: Investigating the internal structure of the Antarctic ice  
867 sheet: the utility of isochrones for spatiotemporal ice-sheet model calibration, *The Cryosphere*, 15,  
868 3839–3860, <https://doi.org/10.5194/tc-15-3839-2021>, 2021.

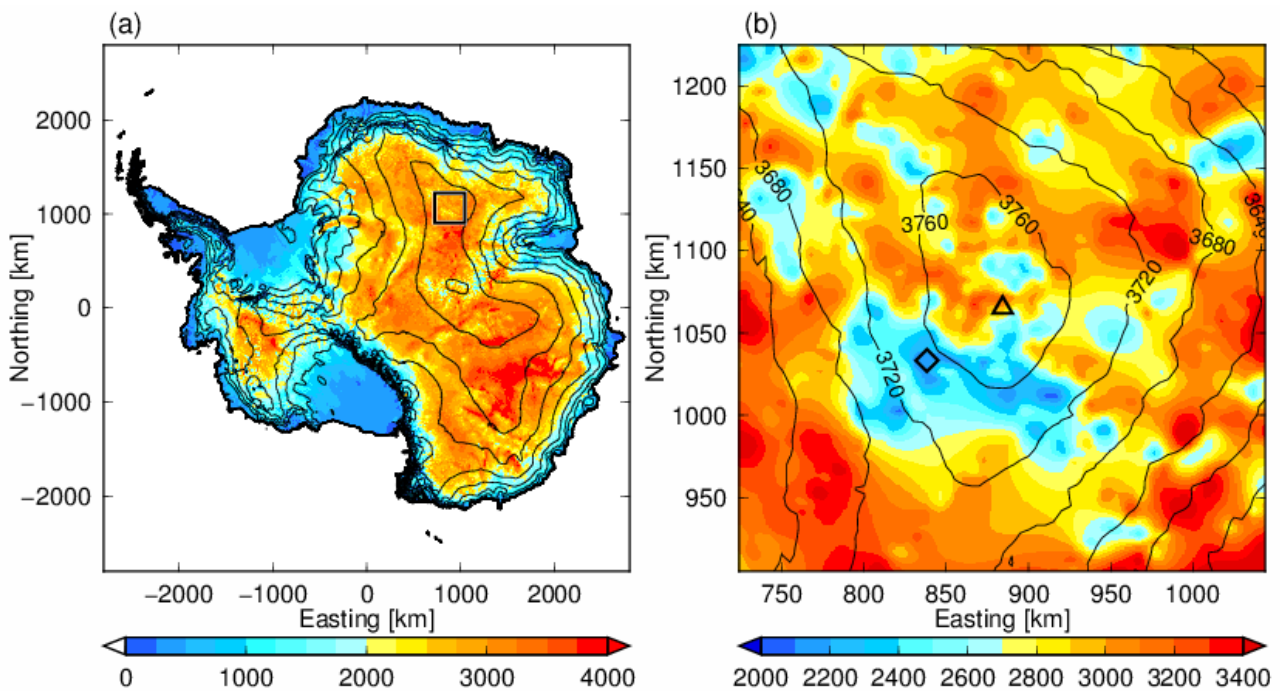
869 ~~48-53.~~ Talalay, P., Li, Y., Augustin, L., Clow, G. D., Hong, J., Lefebvre, E., Markov, A., Motoyama,  
870 H., and Ritz, C.: Geothermal heat flux from measured temperature profiles in deep ice boreholes  
871 in Antarctica, *The Cryosphere*, 14, 4021–4037, <https://doi.org/10.5194/tc-14-4021-2020>, 2020.

872 ~~49-54.~~ Tsutaki, S., Fujita, S., Kawamura, K., Abe-Ouchi, A., Fukui, K., Motoyama, H., Hoshina, Y.,  
873 Nakazawa, F., Obase, T., Ohno, H., Oyabu, I., Saito, F., Sugiura, K., and Suzuki, T.: High-  
874 resolution subglacial topography around Dome Fuji, Antarctica, based on ground-based radar  
875 surveys conducted over 30 years, *The Cryosphere*, 16, 2967-2983, doi: 10.5194/tc-16-2967-2022,  
876 2022

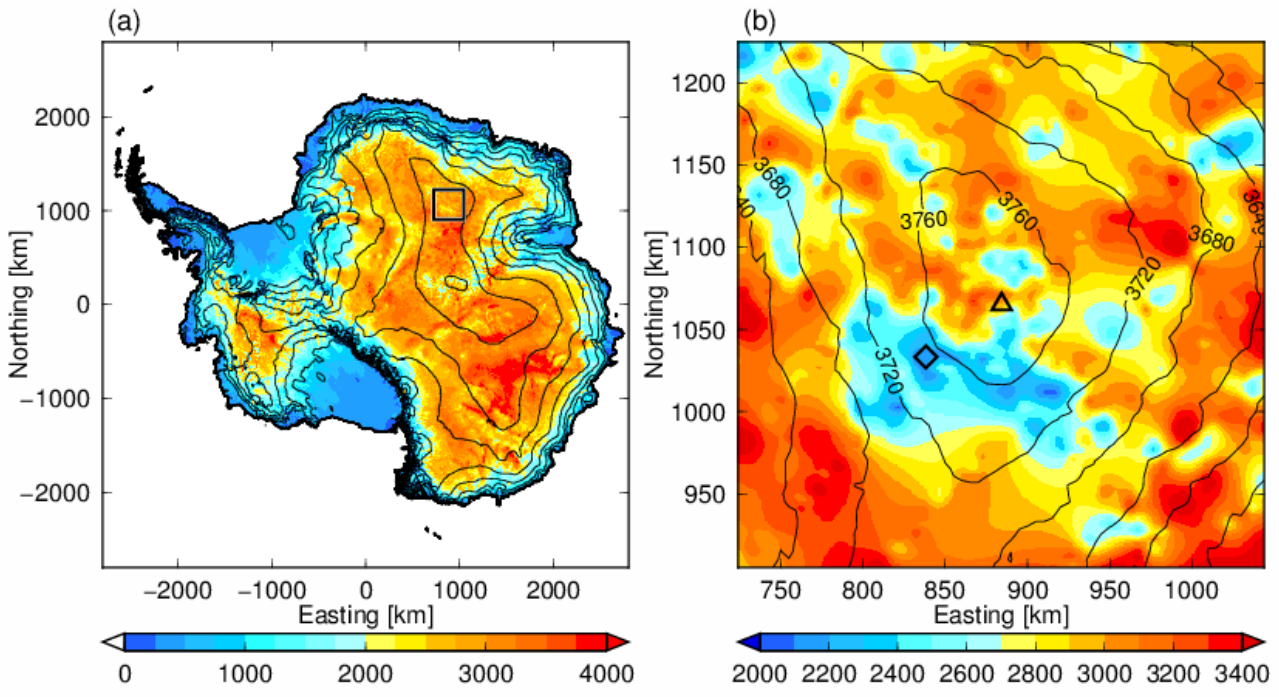
877 ~~50-55.~~ Uemura, R., Motoyama, H., Masson-Delmotte, V., Jouzel, J., Kawamura, K., Goto-Azuma, K.,  
878 Fujita, S., Kuramoto, T., Hirabayashi, M., Miyake, T., Ohno, H., Fujita, K., Abe-Ouchi, A., Iizuka,  
879 Y., Horikawa, S., Igarashi, M., Suzuki, K., Suzuki, T., and Fujii, Y.: Asynchrony between  
880 Antarctic temperature and CO<sub>2</sub> associated with obliquity over the past 720,000 years, *Nat.*  
881 *Commun.*, 9, 961, doi:10.1038/s41467-018-03328-3, 2018.

- 882 [51-56.](#) Van Liefferinge, B. and Pattyn, F.: Using ice-flow models to evaluate potential sites of million  
883 year-old ice in Antarctica, *Clim. Past*, 9, 2335–2345, doi:10.5194/cp-9-2335-2013, 2013.
- 884 [52-57.](#) Van Liefferinge, B., Pattyn, F., Cavitte, M. G. P., Karlsson, N. B., Young, D. A., Sutter, J., and  
885 Eisen, O.: Promising Oldest Ice sites in East Antarctica based on thermodynamical modelling, *The*  
886 *Cryosphere*, 12, 2773–2787, doi:10.5194/tc-12-2773-2018, 2018.
- 887 [53-58.](#) Van Liefferinge, B., Taylor, D., Tsutaki, S., Fujita, S., Gogineni, P., Kawamura, K., et al.,  
888 Surface mass balance controlled by local surface slope in inland Antarctica: Implications for ice-  
889 sheet mass balance and Oldest Ice delineation in Dome Fuji. *Geophysical Research Letters*, 48,  
890 e2021GL094966. doi:10.1029/2021GL094966, 2021.
- 891 [54-59.](#) Veres, D., L. Bazin, A. Landais, H. Toyé Mahamadou Kele, B. Lemieux-Dudon, F. Parrenin,  
892 P. Martinerie, E. Blayo, T. Blunier, E. Capron, J. Chappellaz, S.O. Rasmussen, M. Severi, A.  
893 Svensson, B. Vinther, and E.W. Wolff, The Antarctic ice core chronology (AICC2012): an  
894 optimized multi-parameter and multi-site dating approach for the last 120 thousand years, *Climate*  
895 *of the Past*, 9, 1733-1748, doi: 10.5194/cp-9-1733-2013, 2013.
- 896 [55-60.](#) Yamanouchi, T., Hirasawa, N., Hayashi, M., Takahashi, S., Kaneto S.: Meteorological  
897 characteristics of Antarctic inland station, Dome Fuji, *Memoirs of National Institute of Polar*  
898 *Research*. Special issue 57, 94-104, 2003
- 899 [56-61.](#) Young, D. A., Roberts, J. L., Ritz, C., Frezzotti, M., Quartini, E., Cavitte, M. G. P., Tozer, C.  
900 R., Steinhage, D., Urbini, S., Corr, H. F. J., van Ommen, T., and Blankenship, D. D.: High-  
901 resolution boundary conditions of an old ice target near Dome C, Antarctica, *The Cryosphere*, 11,  
902 1897–1911, <https://doi.org/10.5194/tc-11-1897-2017>, 2017
- 903 [57-62.](#) Zhao, L., Moore, J. C., Sun, B., Tang, X., and Guo, X.: Where is the 1-million-year-old ice at  
904 Dome A?, *The Cryosphere*, 12, 1651–1663, doi:10.5194/tc-12-1651-2018, 2018.

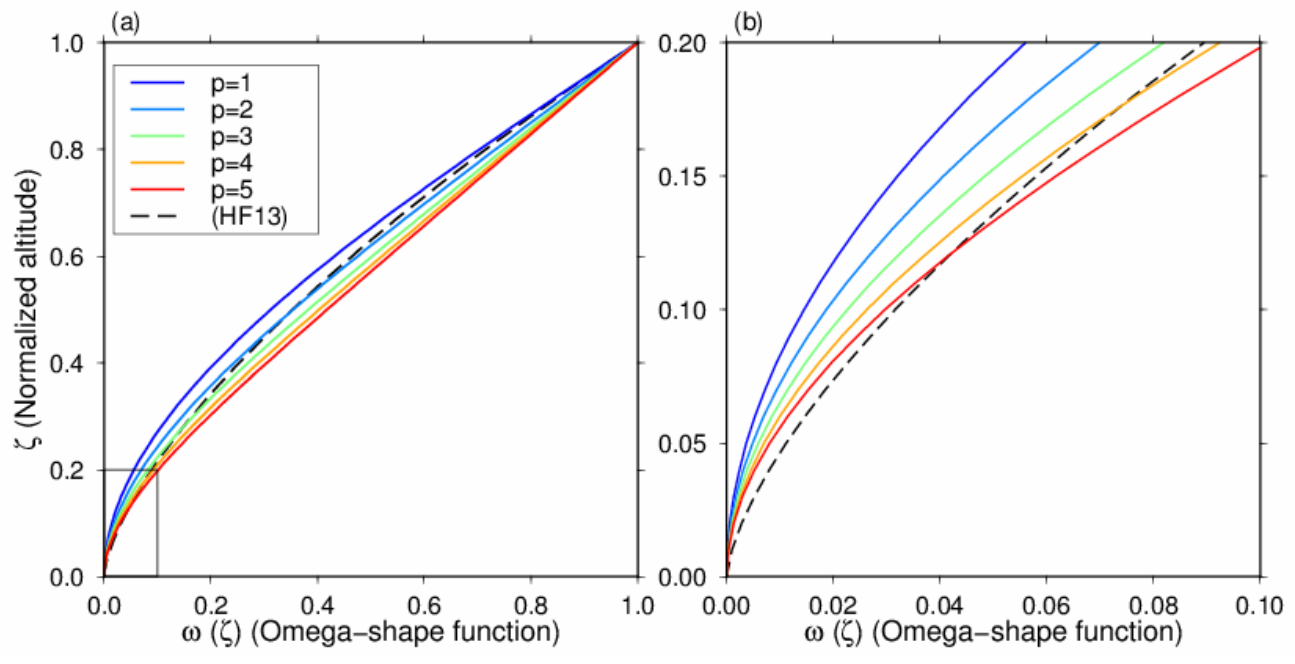
905



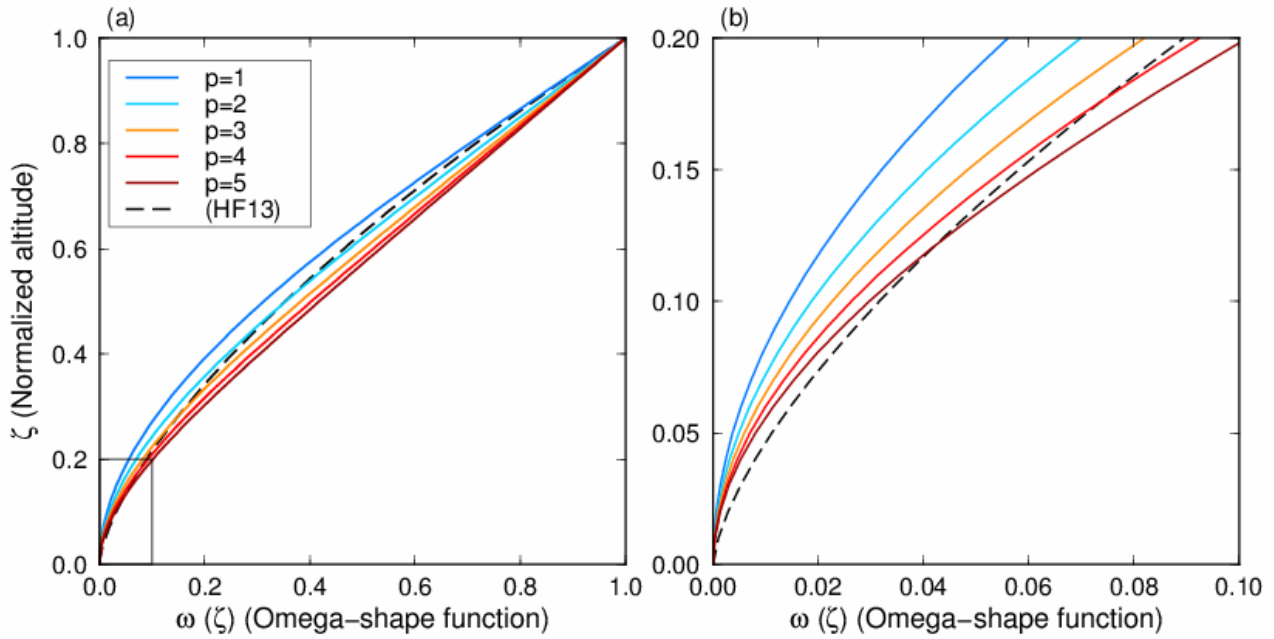
906



907  
 908 Fig. 1: (a) Map of Antarctica. The contours (every 500 m) indicate the surface elevation, and colors  
 909 indicate ice thickness, using BEDMAP2 (Fretwell et al., 2013). The square indicates the location of  
 910 the inset shown in (b). (b) Enlarged view near DF (Dome Fuji). The triangle indicates the location of  
 911 the DF ice core site, and the diamond indicates the NDF site.



912

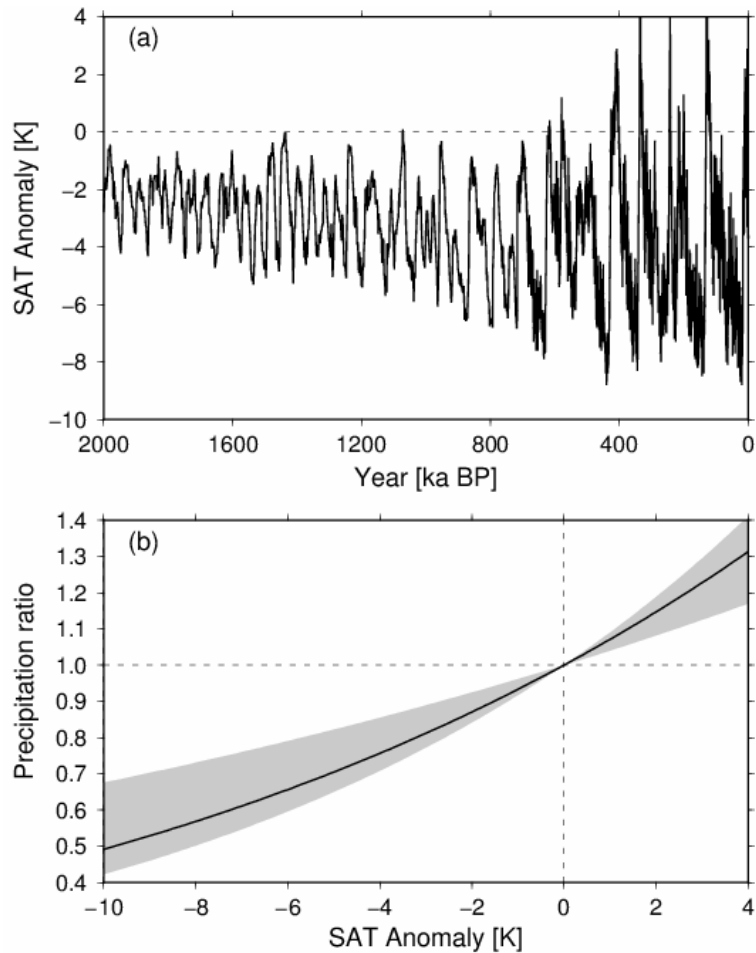


913

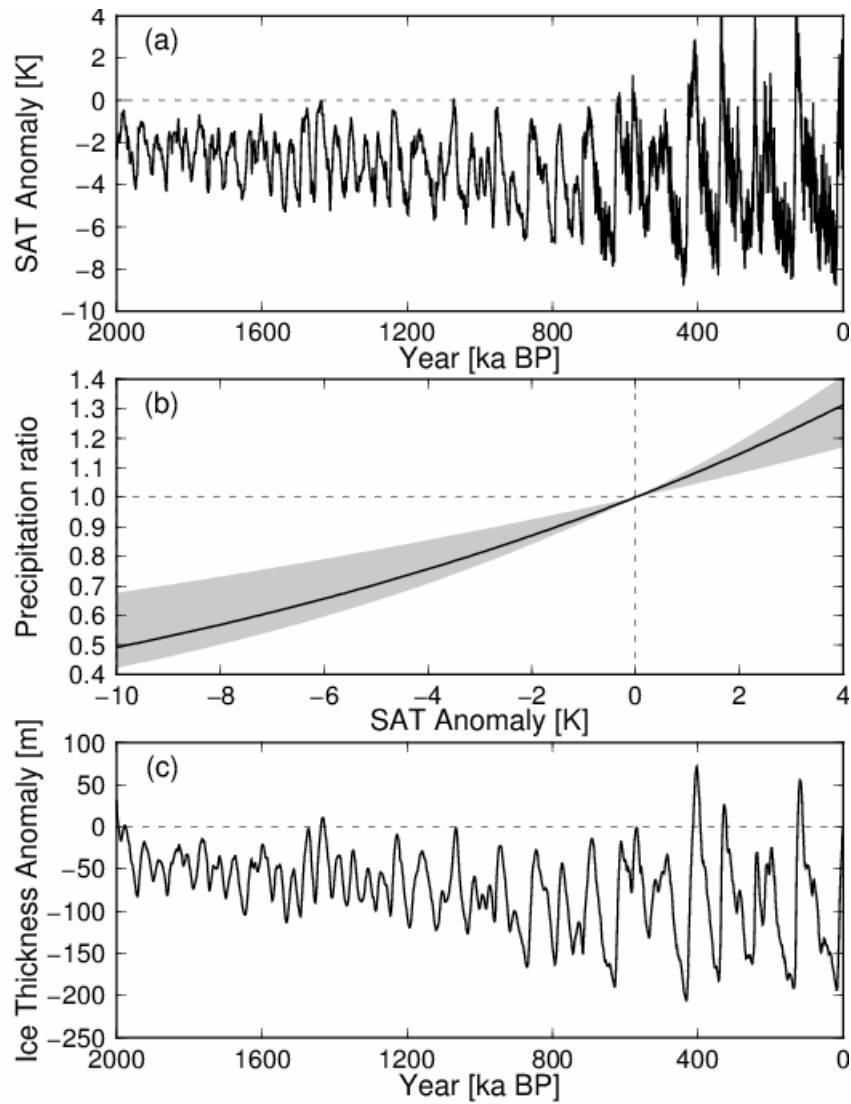
914 **Fig. 2:** (a) Normalized vertical velocity profiles adopted from Equation [43] with different  $p$  parameters.  
 915 The dashed black line (HF13) indicates the vertical velocity profile used in Fischer et al. (2013) with  
 916  $m = 0.5$ . (b) Enlarged view near the bottom of the ice column (see black rectangle in (a)).

917

918



919



920

921

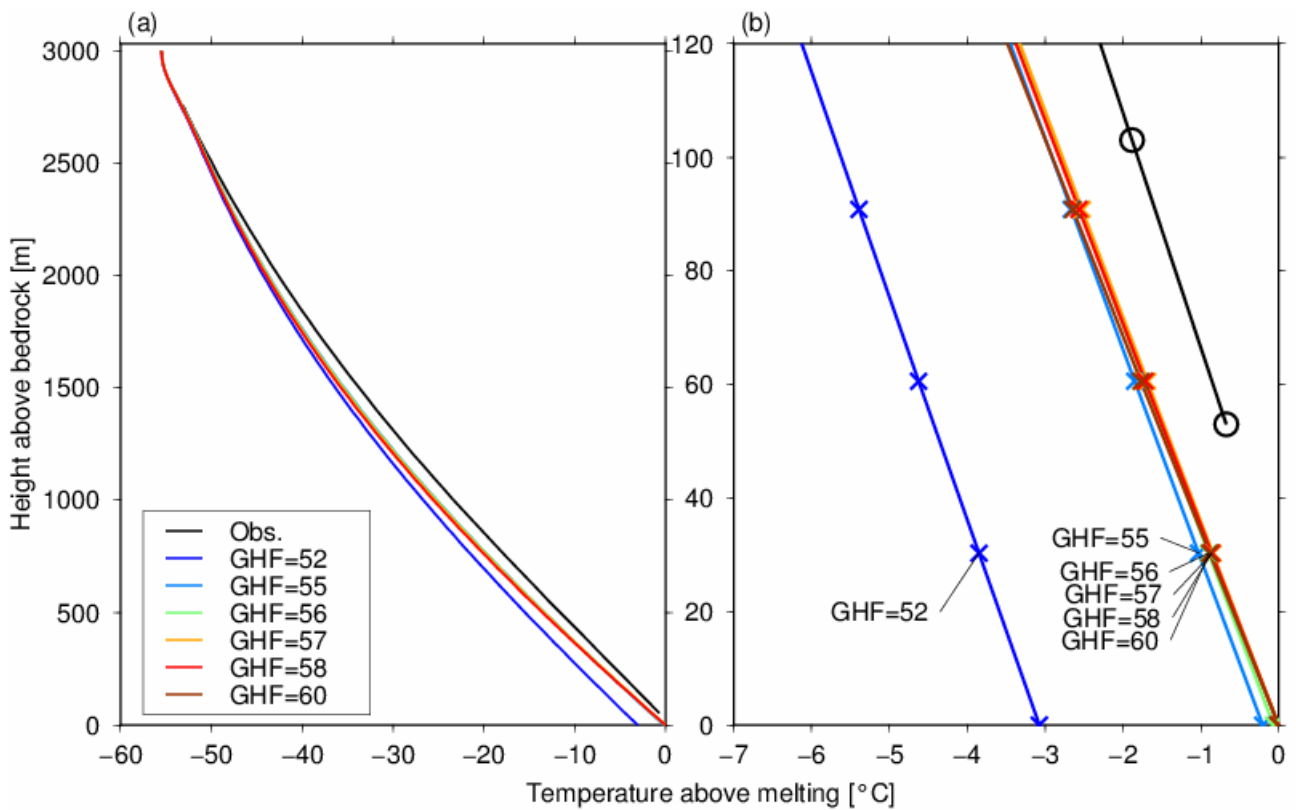
922

923

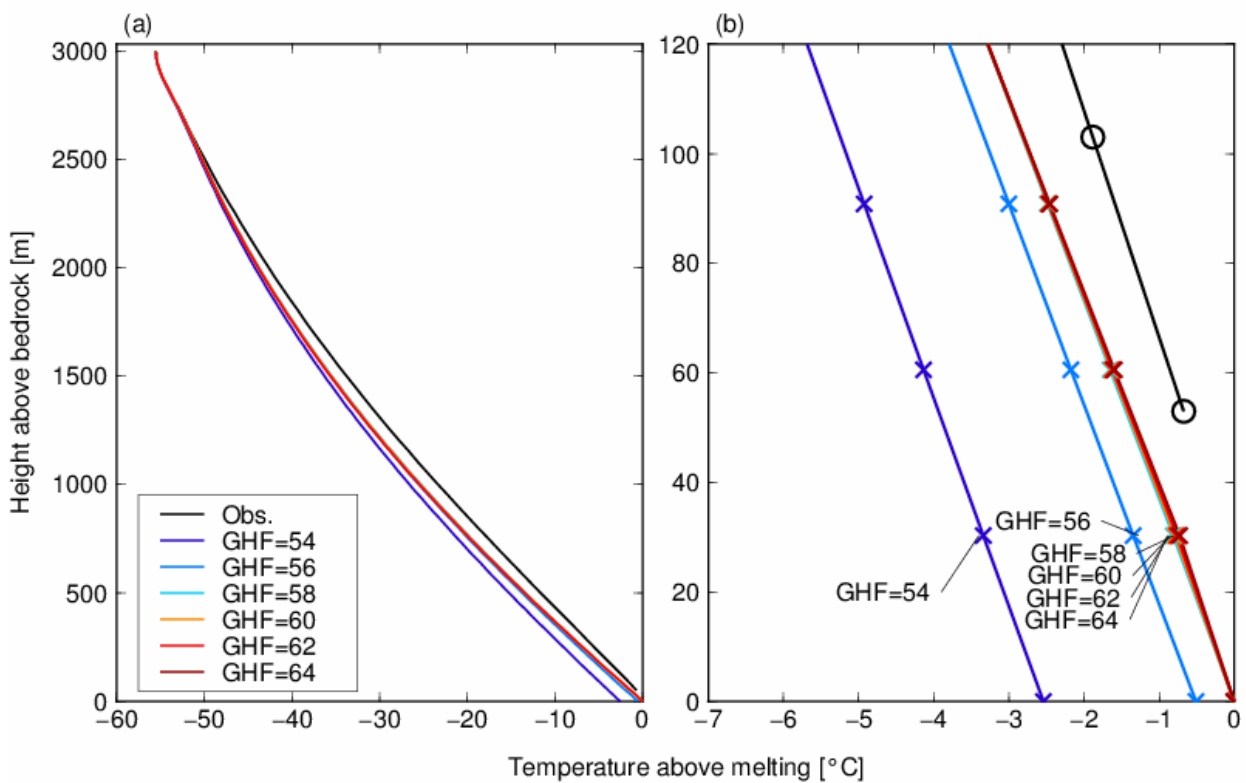
924

925

Fig. 3: Glacial cycle forcing used in the present study. (a) Surface air temperature (SAT) anomaly from the present day for the last 2 Ma. (b) Relationship between SAT anomaly and precipitation ratio. The black line corresponds to the [relationship](#) used in the present study; the gray shading indicates a 4%–9% increase per degree, summarized in Fox-Kemper et al. (2021). (c) [Ice thickness anomaly at DF from a 3-D ice sheet model in the present study.](#)

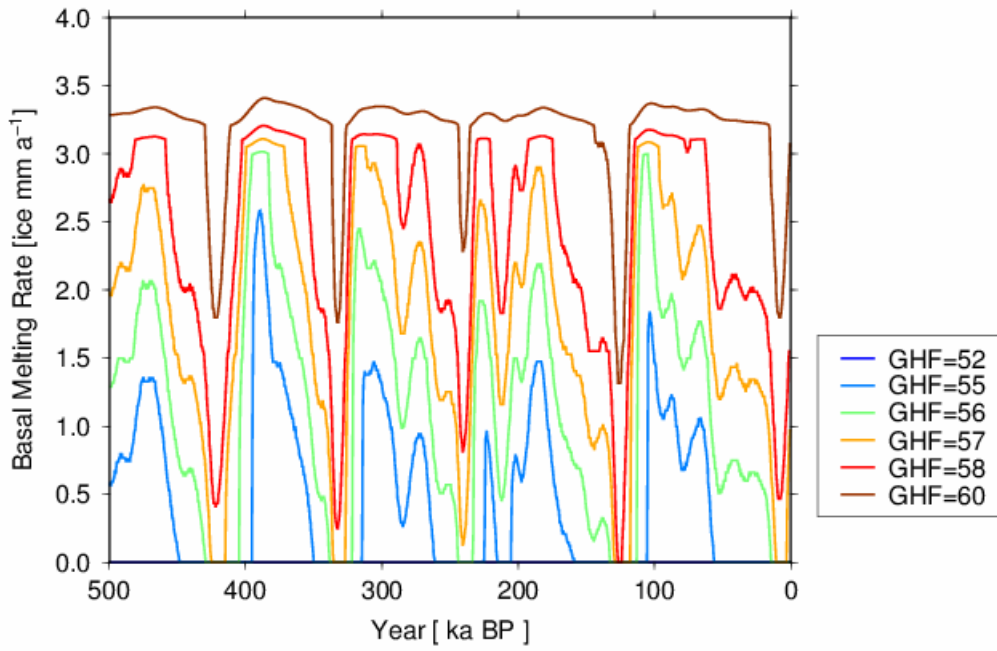


926

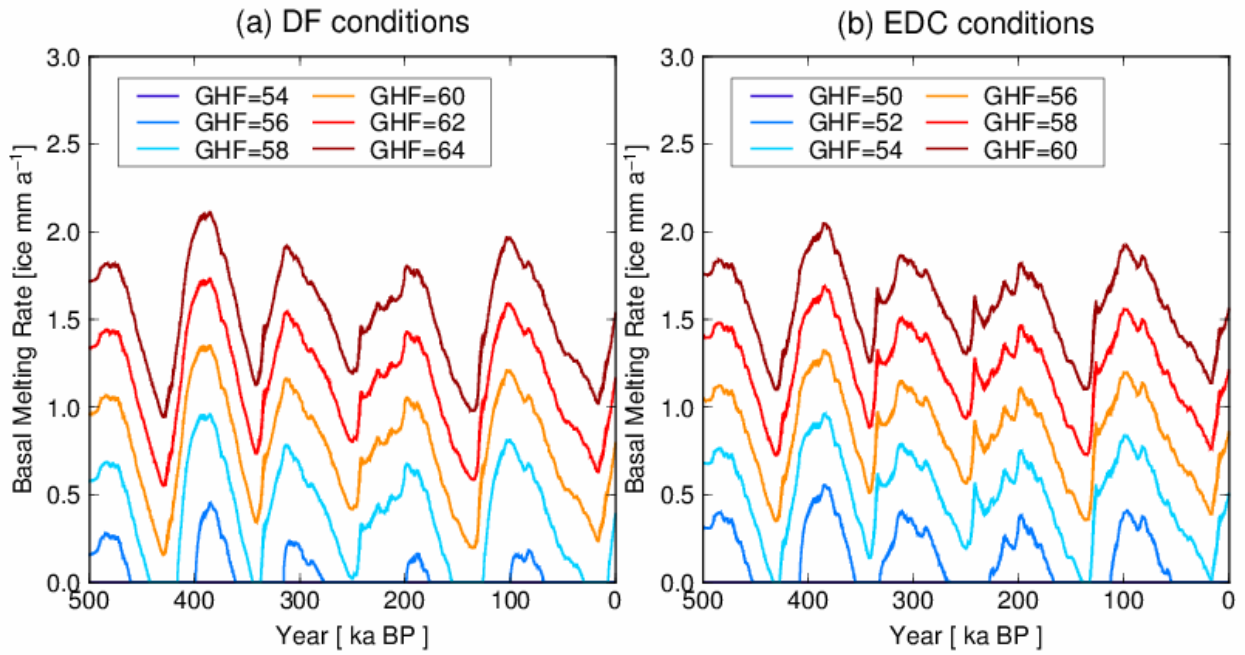


927

928 **Fig. 4:** Simulated vertical temperature profiles under the DF configuration (Table 1) with different  
 929 geothermal heat fluxes (GHF; units are  $\text{mW m}^{-2}$ ). (a) Simulated temperature profiles at 0 ka (end of  
 930 the simulation) from the surface to the base. (b) Close-up of (a) for the bottom 120 m of the ice column.  
 931 The black lines represent the measured temperature profiles and the black circles in (b) indicate the  
 932 location of data points, while the colored crosses in (b) represent the model grid points.



933



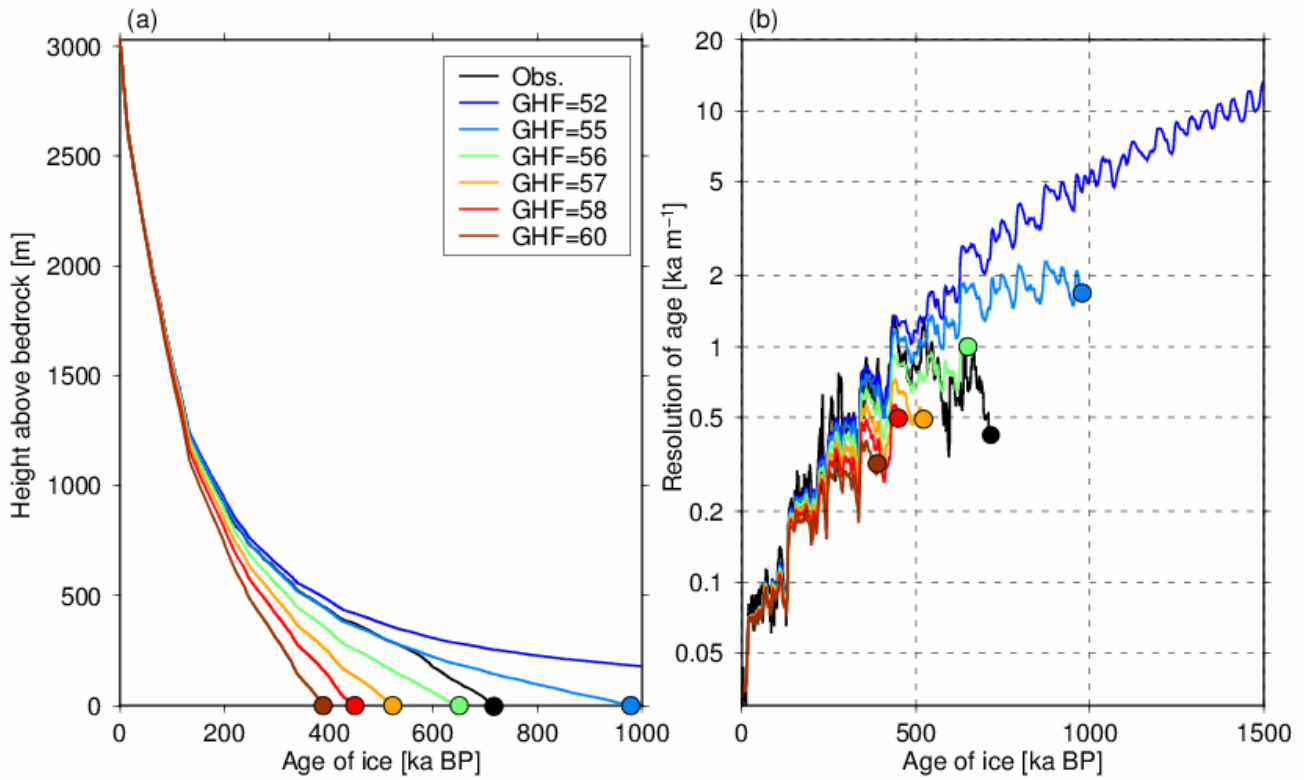
934

935

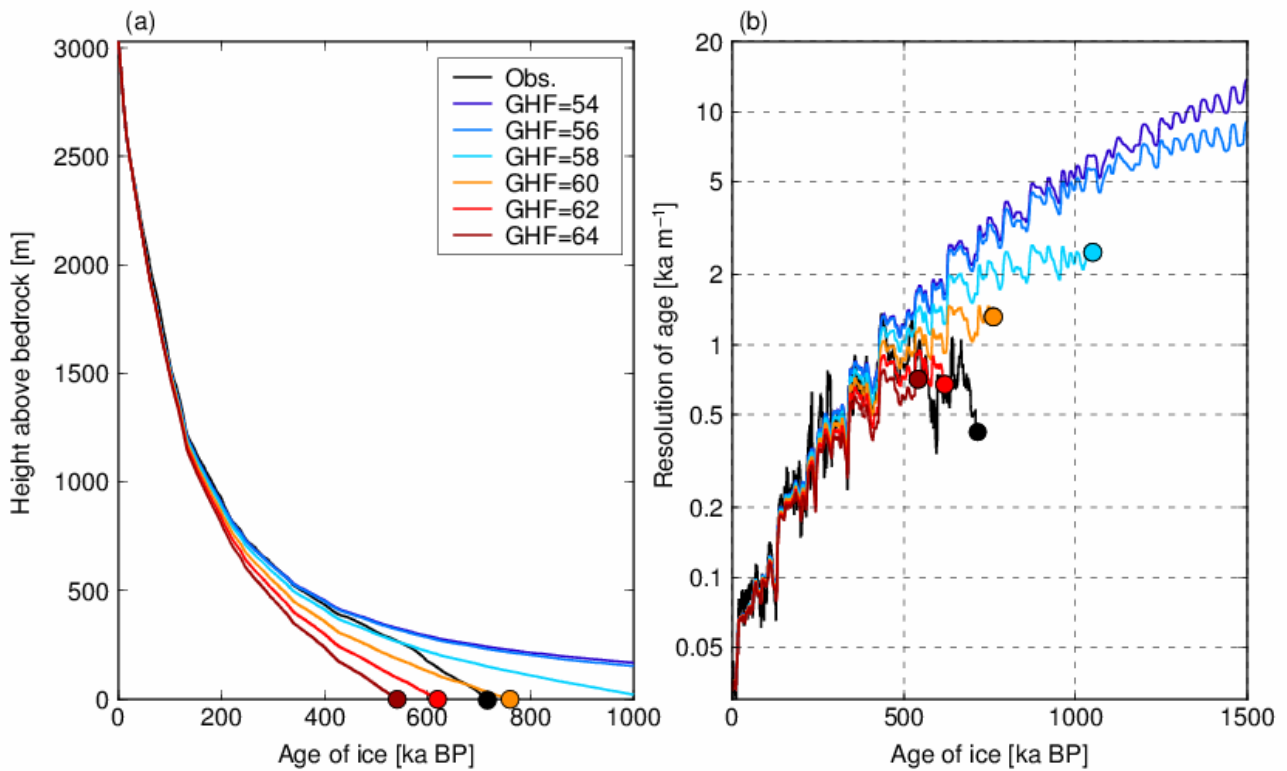
936

Fig. 5: Time series of the simulated basal melting rates of the last 500 ka under the DF configuration and EDC configurations (Table 1) with different geothermal heat fluxes (GHF; units are  $\text{mW m}^{-2}$ ).



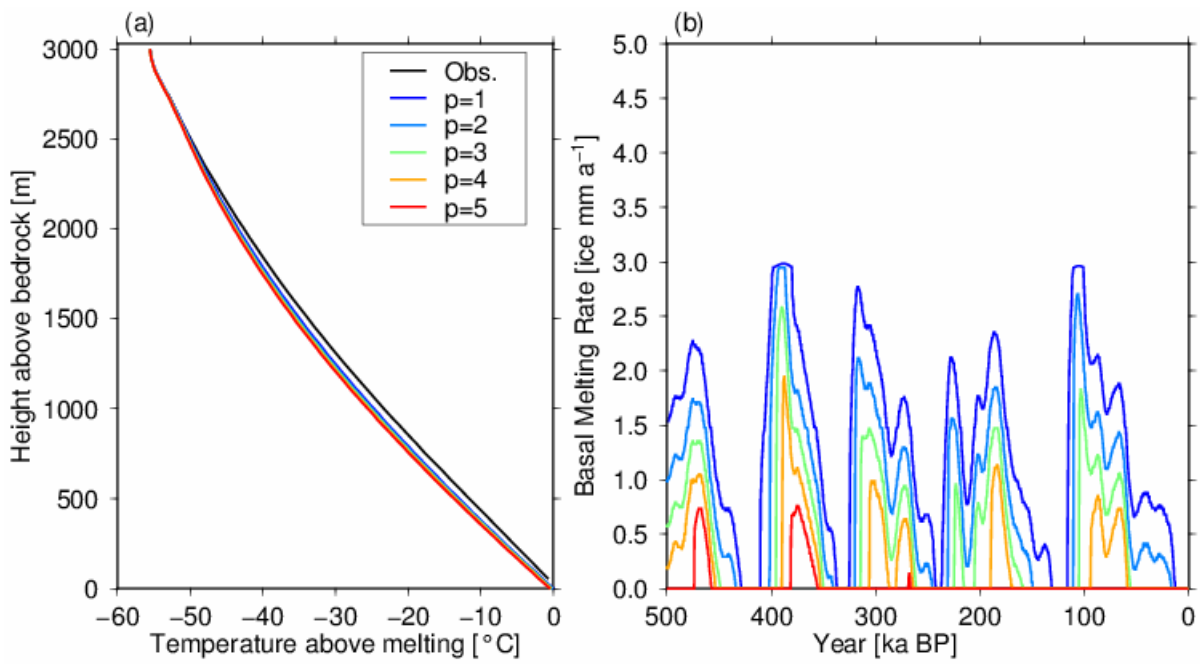


937



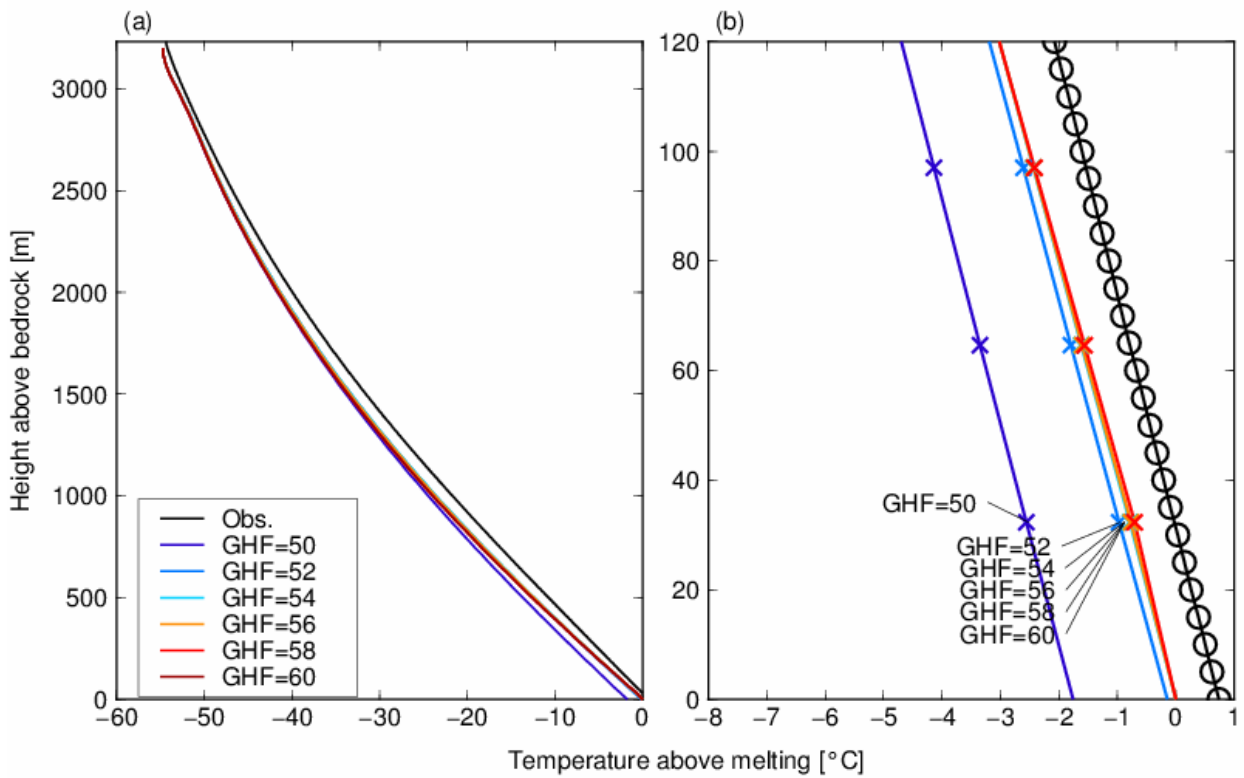
938

939 Fig. 6: Simulated vertical ice age profiles under the DF configuration (Table 1) with different  
 940 geothermal heat fluxes (GHF; units are  $\text{mW m}^{-2}$ ). (a) Vertical age profiles at present (0 ka). The black line  
 941 represents the reconstructed depth–age profile based on the AICC2012 chronology (Kawamura et  
 942 al., 2017). The circles indicate the bottom of the ice. (b) Vertical resolution of ice age, calculated by  
 943 the central difference using the simulated vertical age profiles of (a).



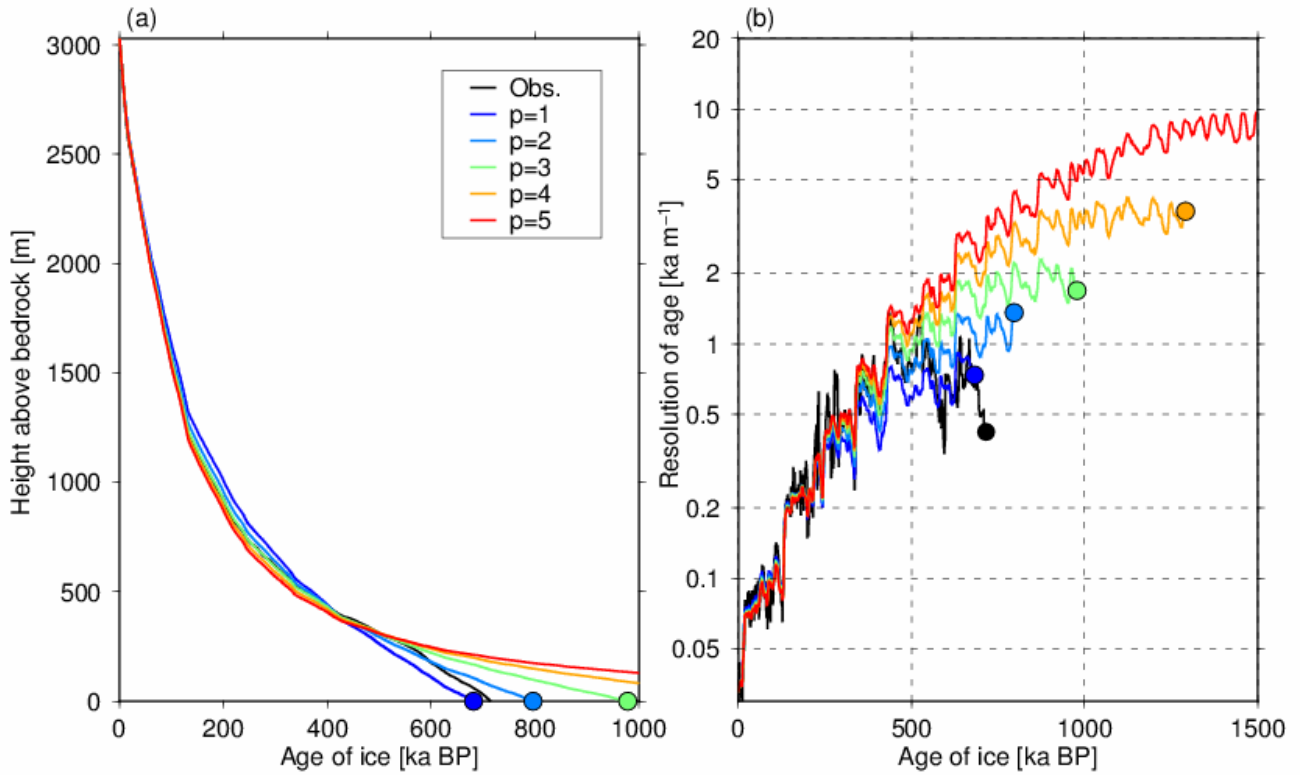
944  
945  
946

Fig. 7: Simulated vertical temperature profiles and basal melting rates under the DF configuration (Table 1) with different  $p$  parameters.



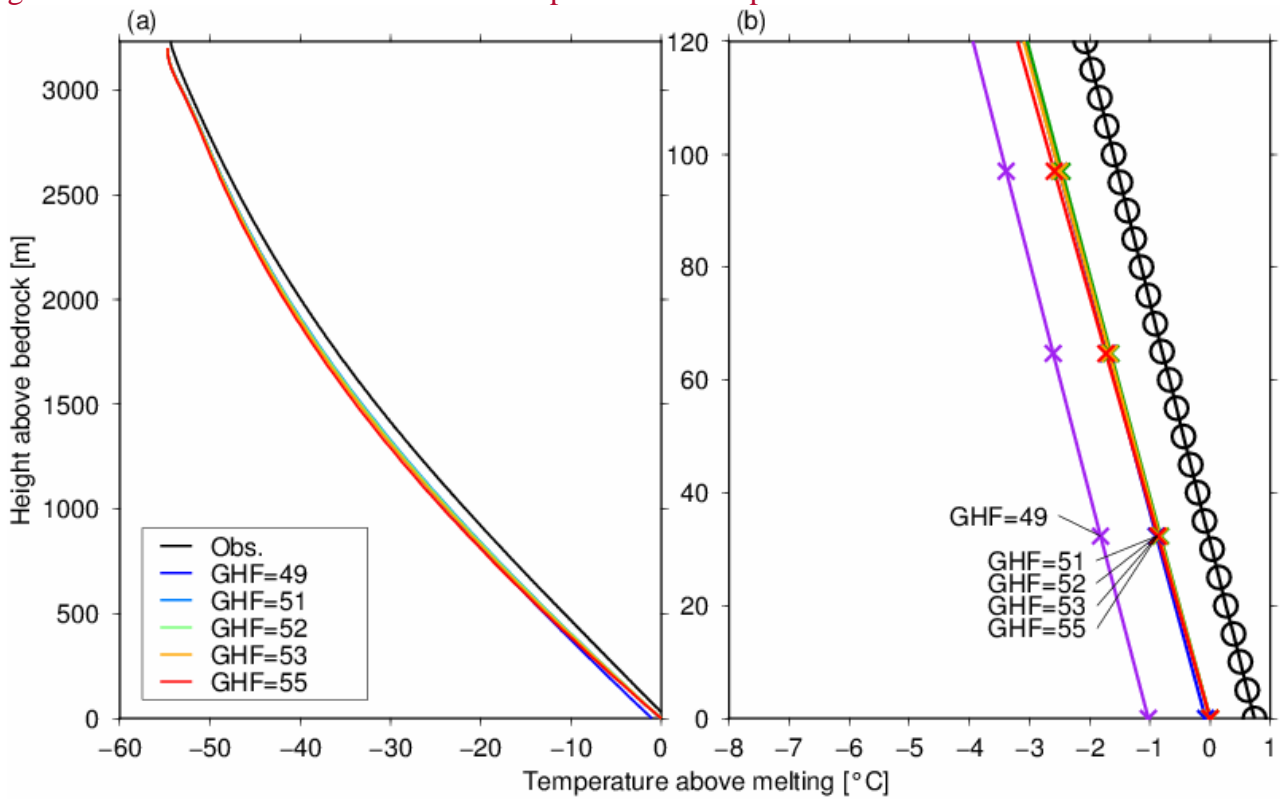
947  
948  
949  
950

Fig. 7(a) Simulated temperature profiles at present (0 ka) from the surface to the base. (b) Time series of basal melting rates over the last 500 ka. A geothermal heat flux of  $55 \text{ mW m}^{-2}$  is adopted in these experiments.



951  
952  
953  
954

Fig. 8: Same as Fig. 6, with different  $p$  parameters. (a) Simulated age profiles at present (0 ka) from the surface to the base. (b) Vertical resolution of ice age. The circles indicate the bottom of the ice. A geothermal heat flux of  $55 \text{ mW m}^{-2}$  is adopted in these experiments.

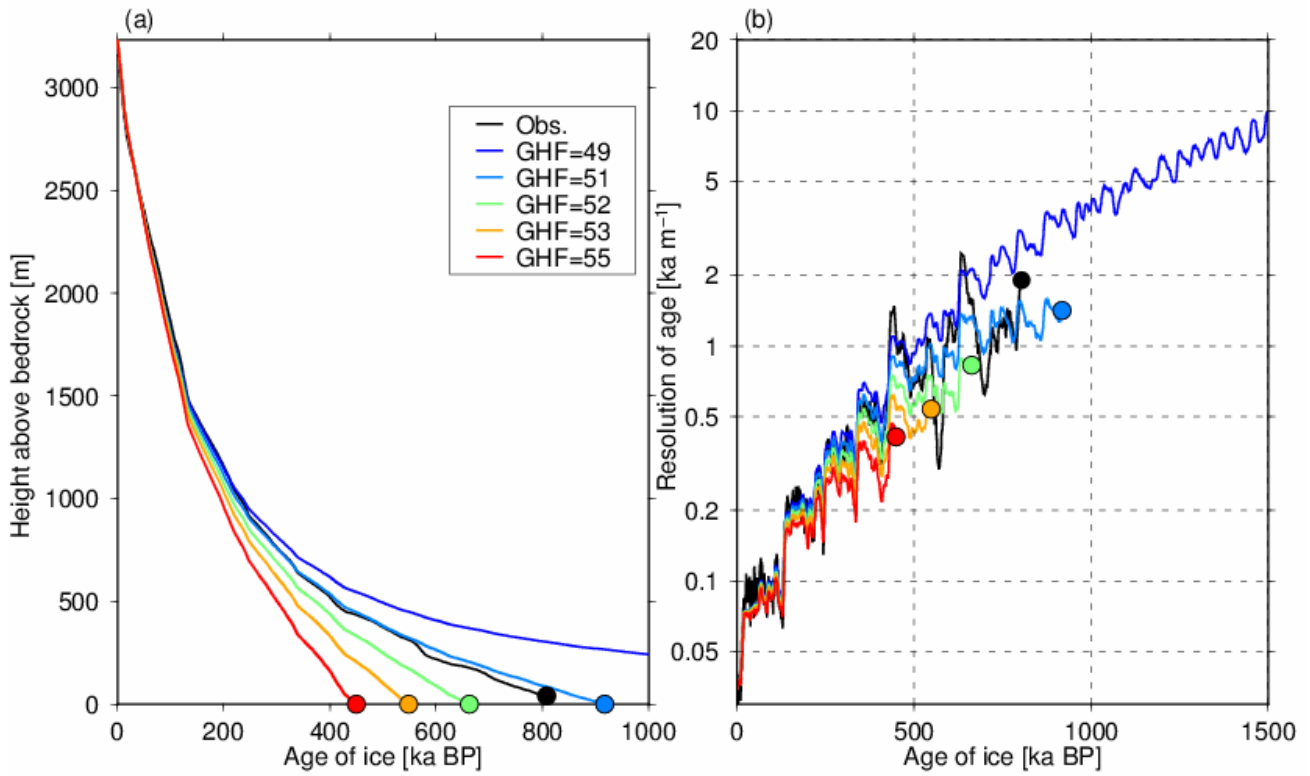


955  
956  
957  
958  
959

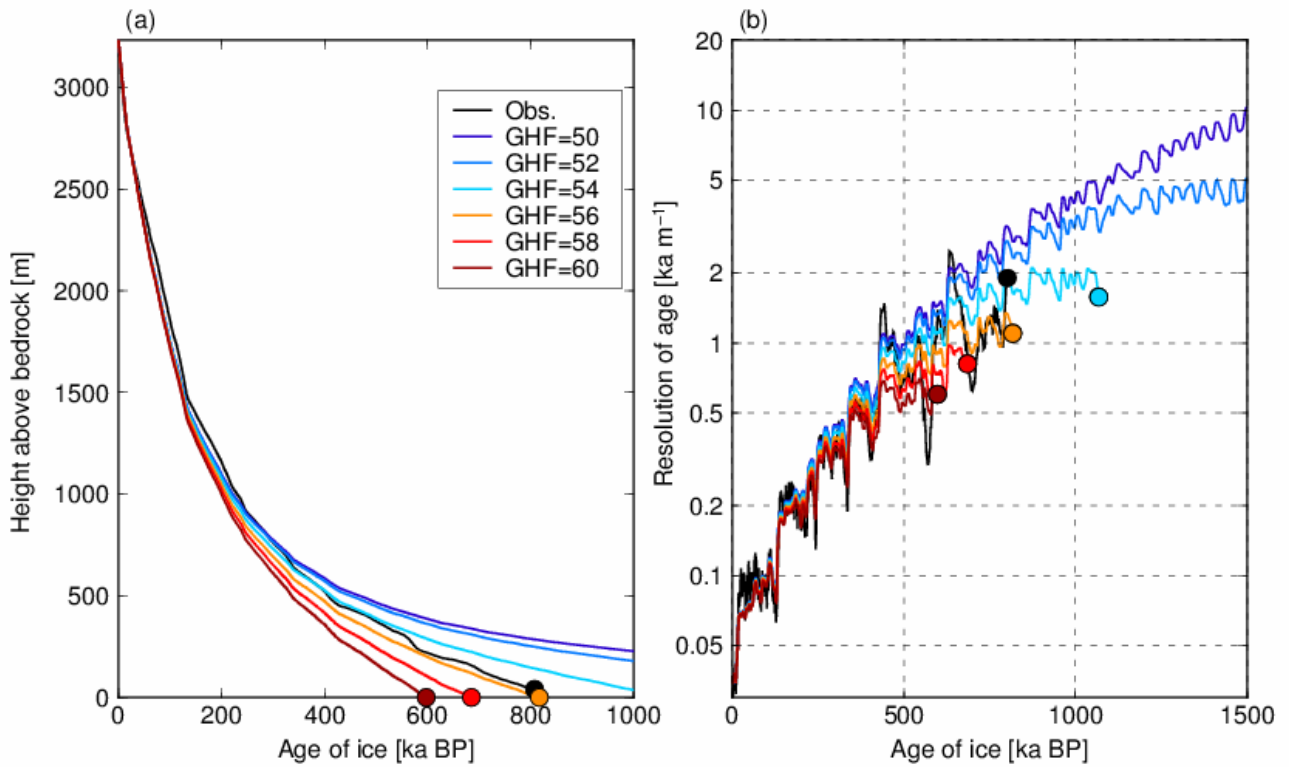
Fig. 9: Same as Fig. 4, but under the EDC configuration (Table 1) with different geothermal heat fluxes (GHF; units are  $\text{mW m}^{-2}$ ). The black lines represent the measured temperature profiles and the black circles in (b) indicate the location of data points, while the colored crosses in (b) represent the model grid points.

960

961



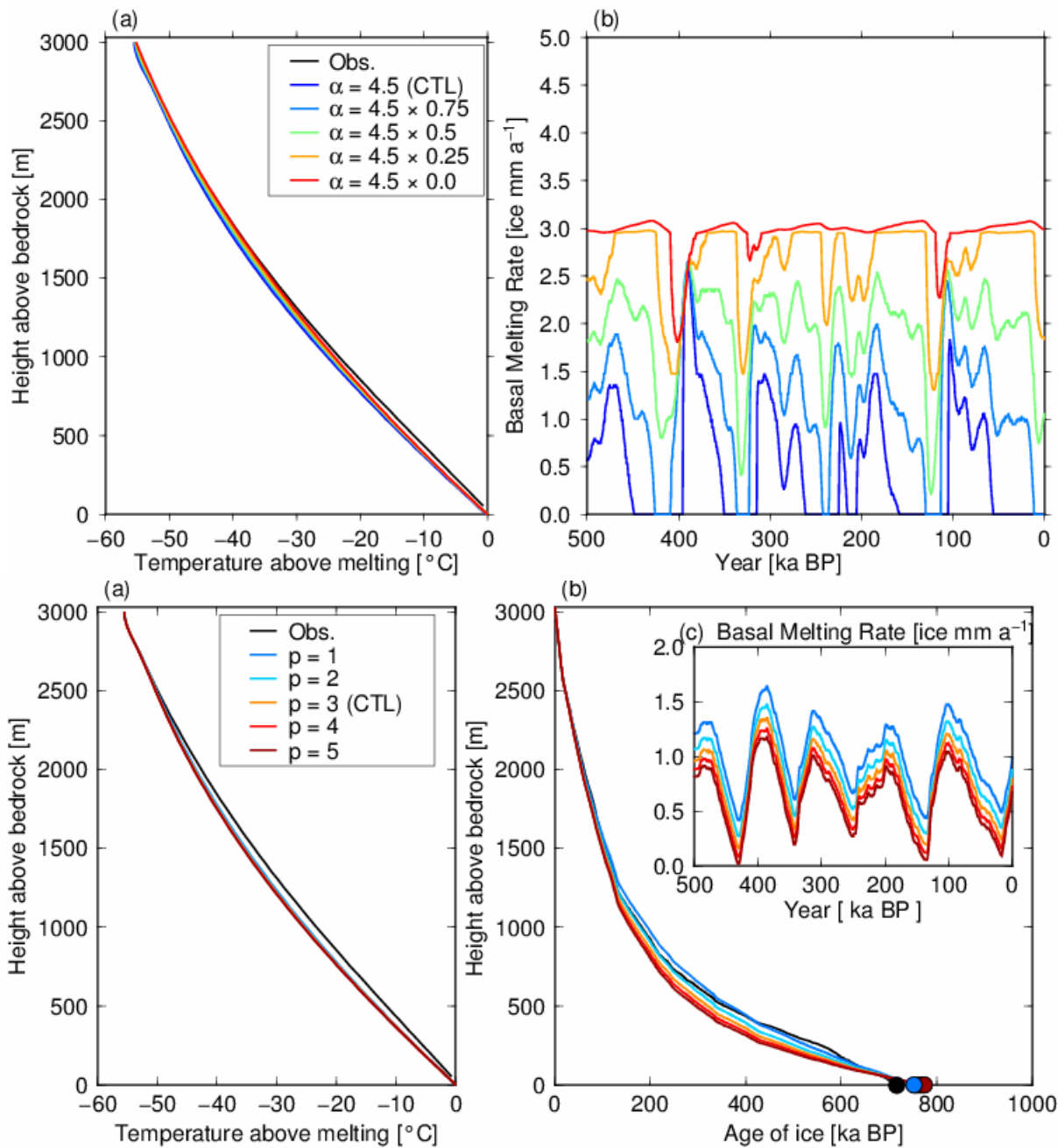
962



963

964 Fig. 108: Same as Fig. 6, but results under the EDC configuration (Table 1). The AICC2012  
965 chronology (Veres et al., 2013) is used in this figure for the observed depth–age profile.

966



967

968

969

970

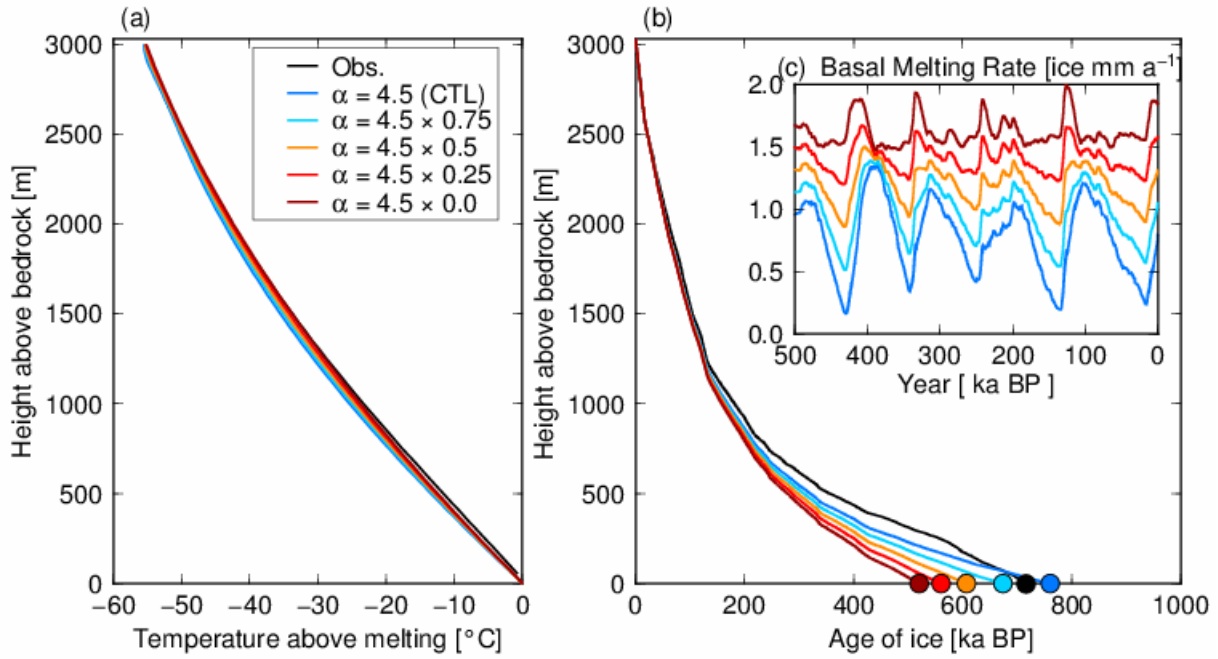
971

972

973

974

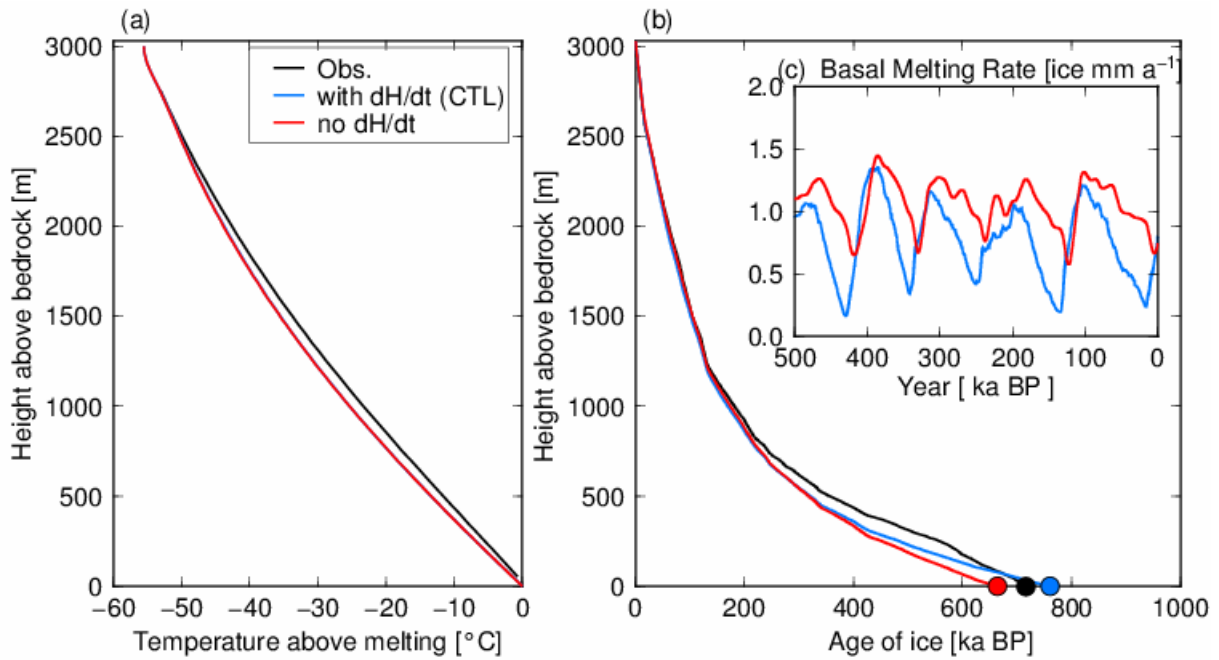
Fig. 11: Simulated vertical temperature profiles and basal melting rates under 9: Results of the DF configuration (Table 1), using with different  $p$  parameters. (a) Simulated temperature profiles at present (0 ka) from the surface to the base. (b) Vertical age profiles at present (0 ka). (c) Time series of basal melting rates over the last 500 ka. A geothermal heat flux of  $60 \text{ mW m}^{-2}$  is adopted in these experiments.



975

976 Fig. 10: Results of the DF configuration (Table 1) with different temperature amplitudes over glacial  
 977 cycles in Equation 810. A combination of  $p = 3$  and  $\text{GHF} = 5560 \text{ mW m}^{-2}$  is adopted in these  
 978 experiments. (a) Simulated temperature profiles at present (0 ka) from the surface to the base. (b)  
 979 Vertical age profiles at present (0 ka). (c) Basal melting rates of the last 500 ka. The dark blue lines  
 980 are the same as the green line of Fig. 4.

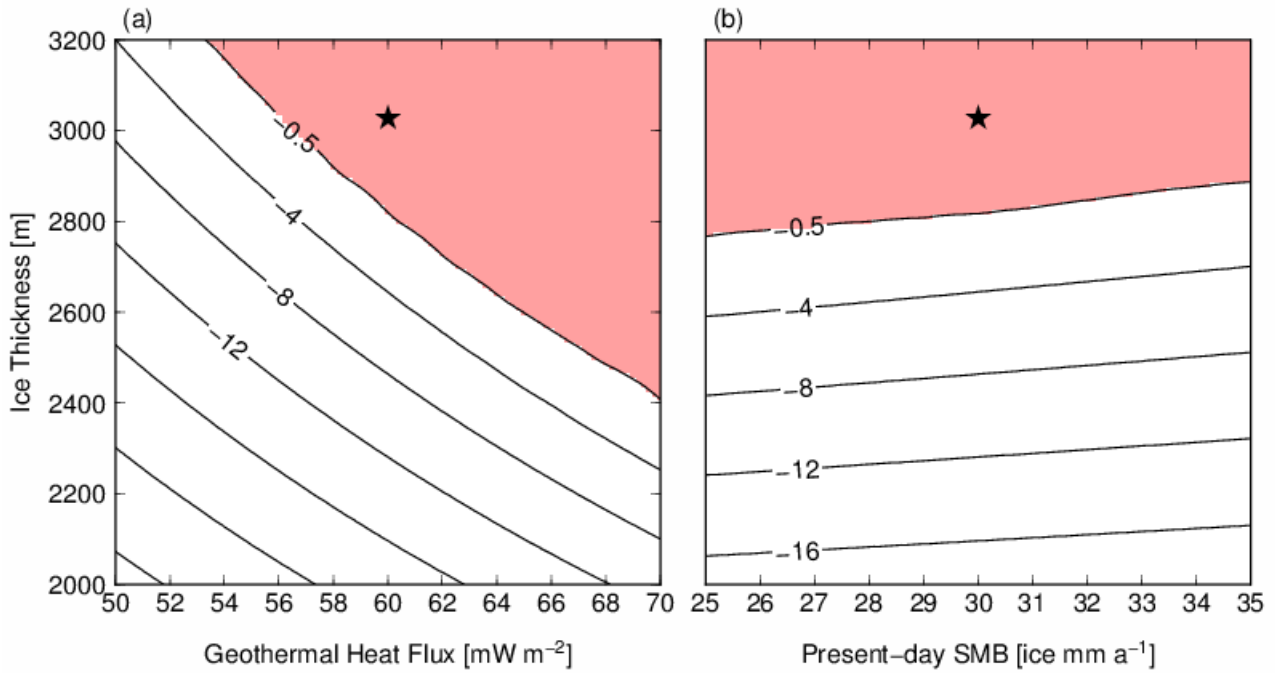
981



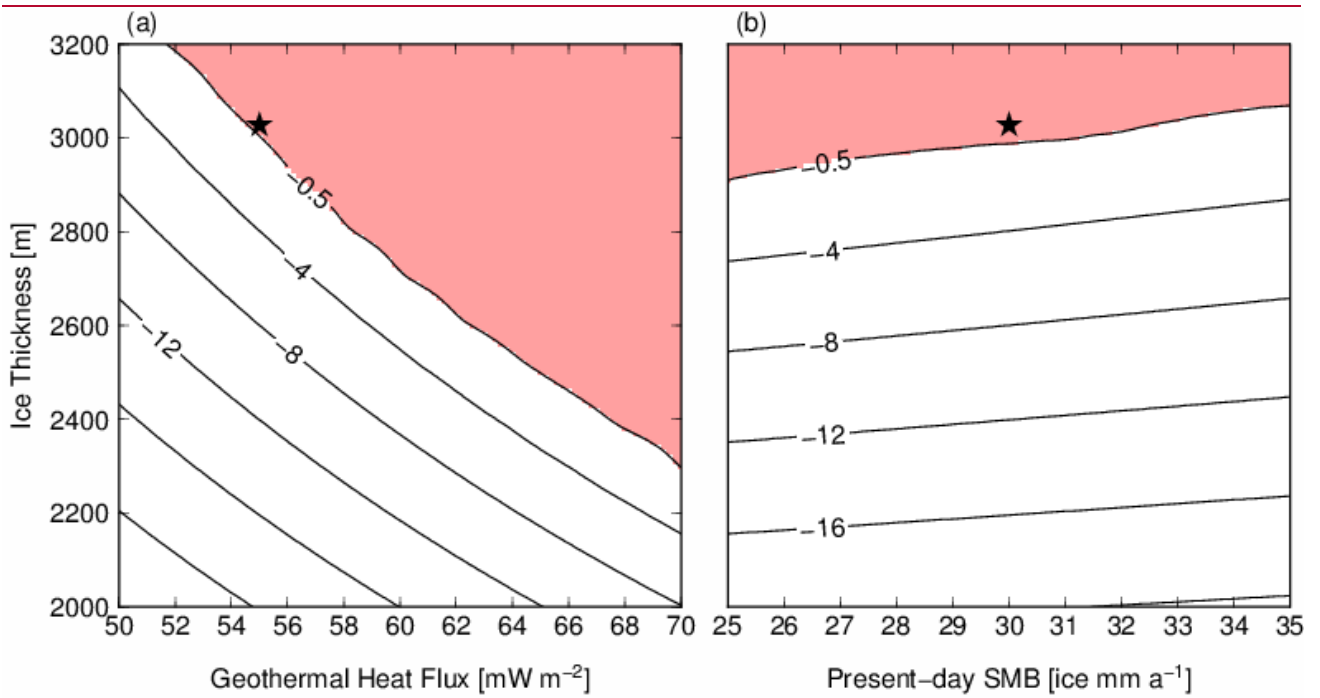
982

983 Fig. 11: Results of the DF configuration (Table 1) with and without ice thickness changes in the past.  
 984 A combination of  $p = 3$  and  $\text{GHF} = 60 \text{ mW m}^{-2}$  is adopted in these experiments. (a) Simulated  
 985 temperature profiles at present (0 ka) from the surface to the base. (b) Vertical age profiles at present  
 986 (0 ka). (c) Basal melting rates of the last 500 ka.

987



988



989

990

991

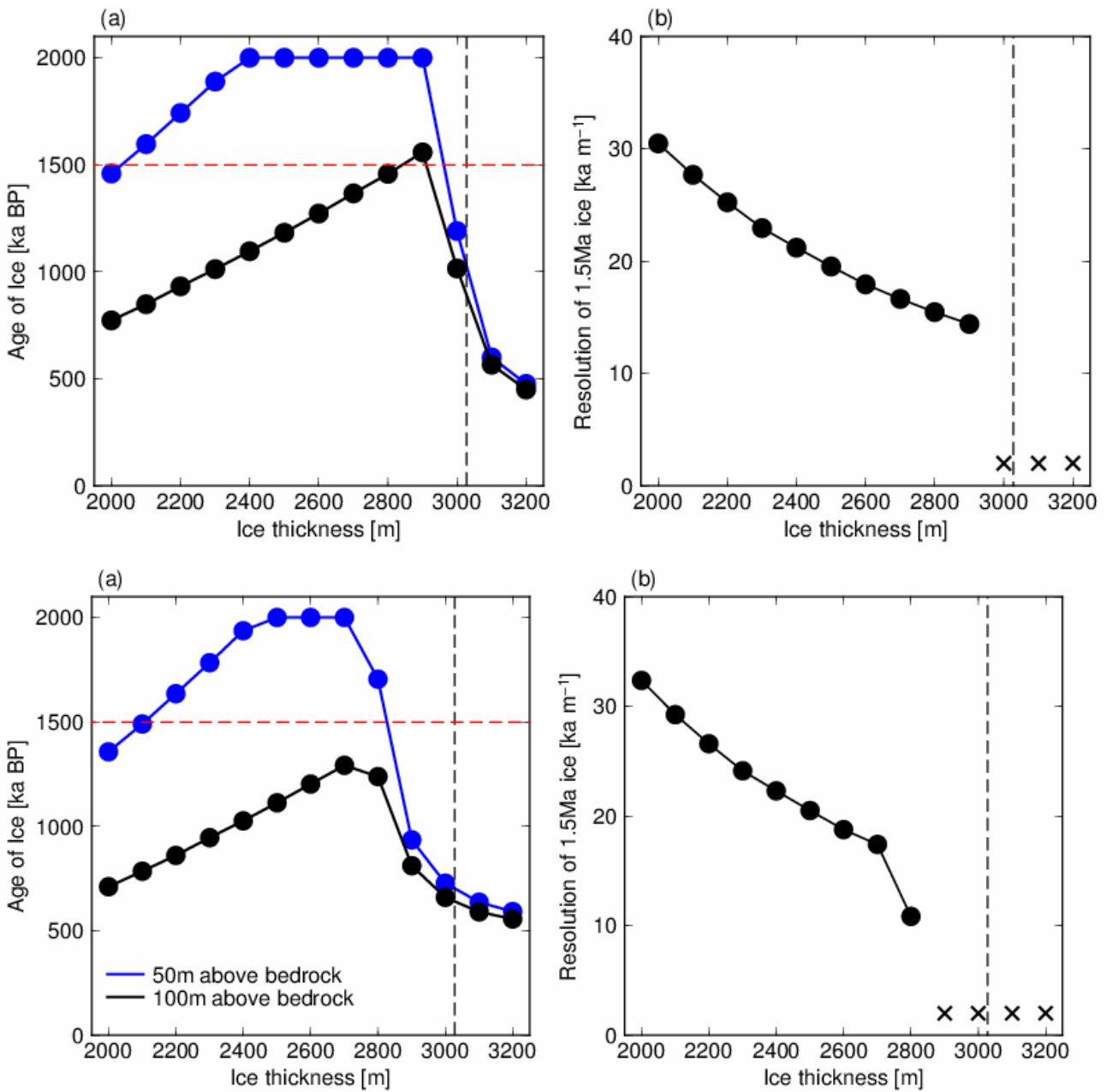
992

993

994

995

Fig. 12: Simulated basal temperature at the present day with combinations of ice thickness, geothermal heat flux, and present-day SMB. (a) Red shading indicates a basal temperature  $-0.5\text{ }^{\circ}\text{C}$  below the pressure-melting point. (b) Basal temperature at the present day with  $\text{GHF} = 55.60\text{ mW m}^{-2}$ . The black star represents the condition at the DF ice core ( $H = 3028\text{ m}$ ,  $\text{SMB} = 30\text{ ice mm a}^{-1}$ ), with a calibrated geothermal heat flux ( $55.60\text{ mW m}^{-2}$ ).



996

997

998

999

1000

1001

1002

1003

Fig. 13: Results with different ice thicknesses: at the DF configuration ( $SMB = 30$  ice equivalent  $mm a^{-1}$  and  $GHF = 60 mW m^{-2}$ ). (a) The black and blue lines indicate the simulated ageages of the ice at 100 and 50 m above the bedrock, respectively. The vertical dashed line ( $H = 3028$  m) indicates the condition at DF, and the horizontal red dashed line indicates the age of 1.5 Ma. Note that an age of 2 Ma is the limit of the experiments. (b) The vertical axis indicates the resolution of the ice age ( $ka m^{-1}$ ) at 1.5 Ma BP. The crosses indicate that the 1.5 Ma age of ice does not exist under these conditions.



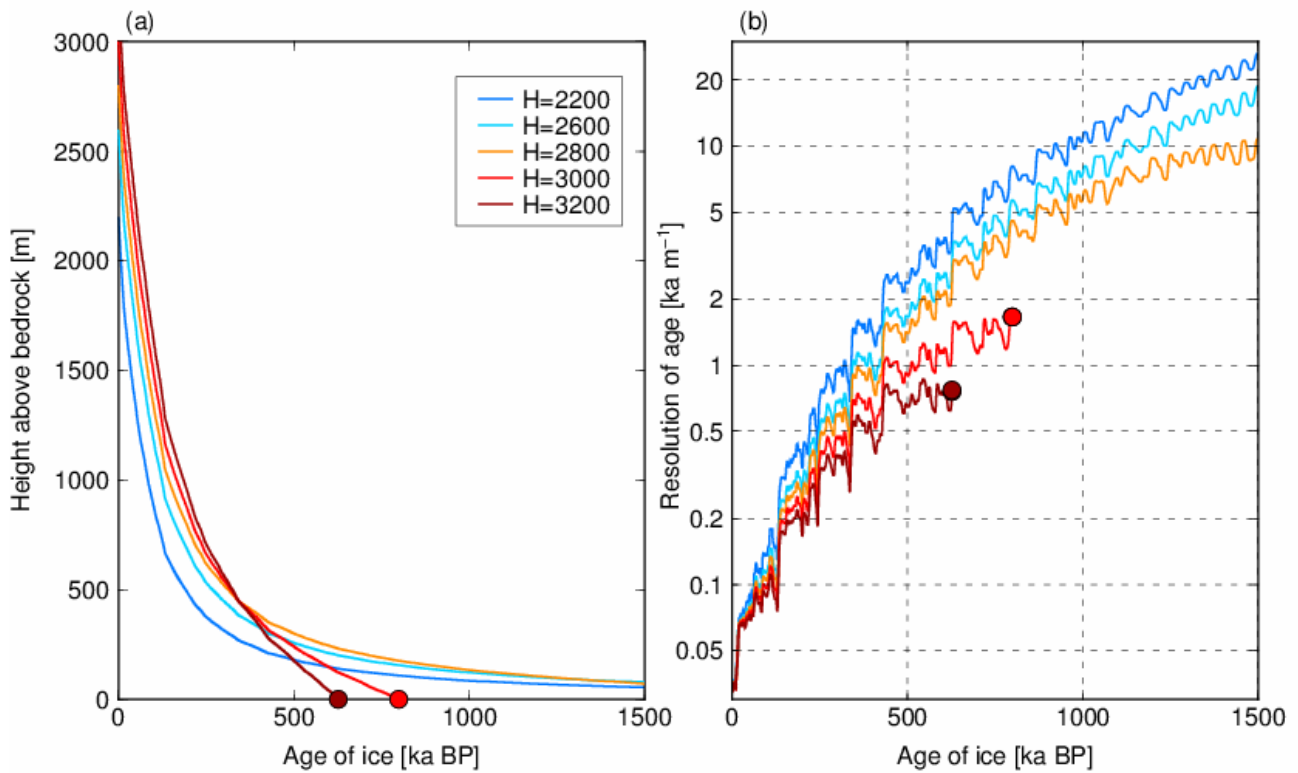
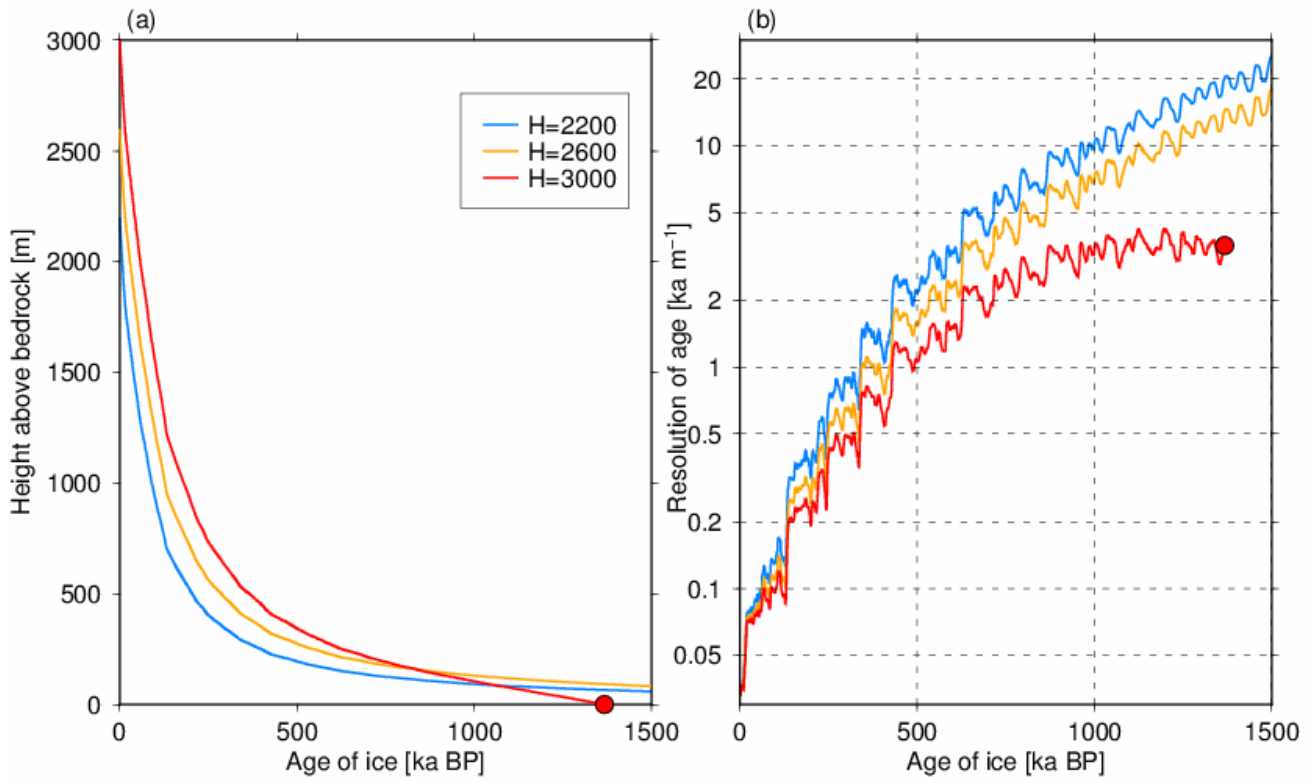


Fig. 14: Results with different ice thicknesses (2200, 2600, 2800, 3000, and 3200 m) with calibrated geothermal heat flux ( $60 \text{ mW m}^{-2}$ ) and SMB ( $55 \text{ mW m}^{-2}$ , 30 ice equivalent  $\text{mm a}^{-1}$ ) at DF. (a) Vertical age profiles (the circle on the H = 3000 m case indicates the bottom of the ice) at present (0 ka). (b) Vertical resolution of the ice age.

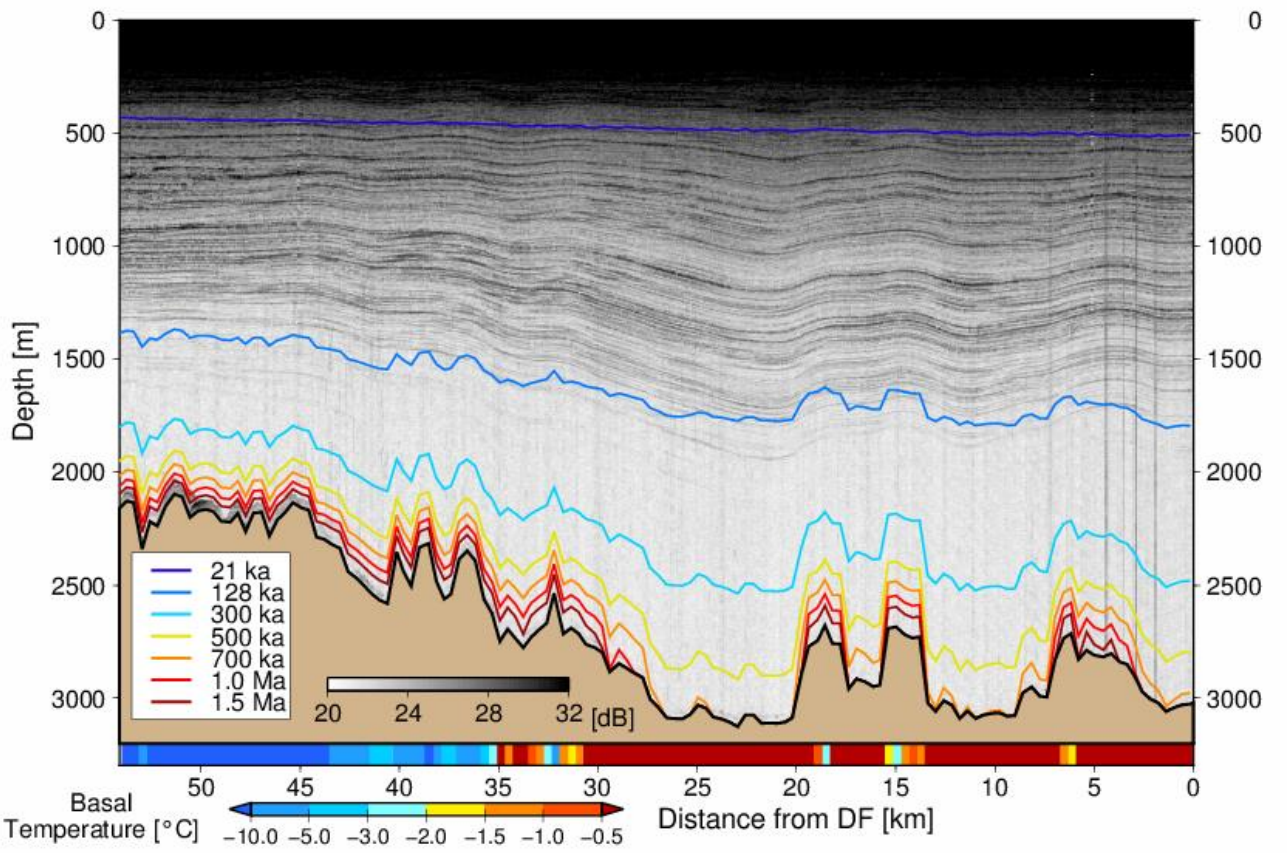
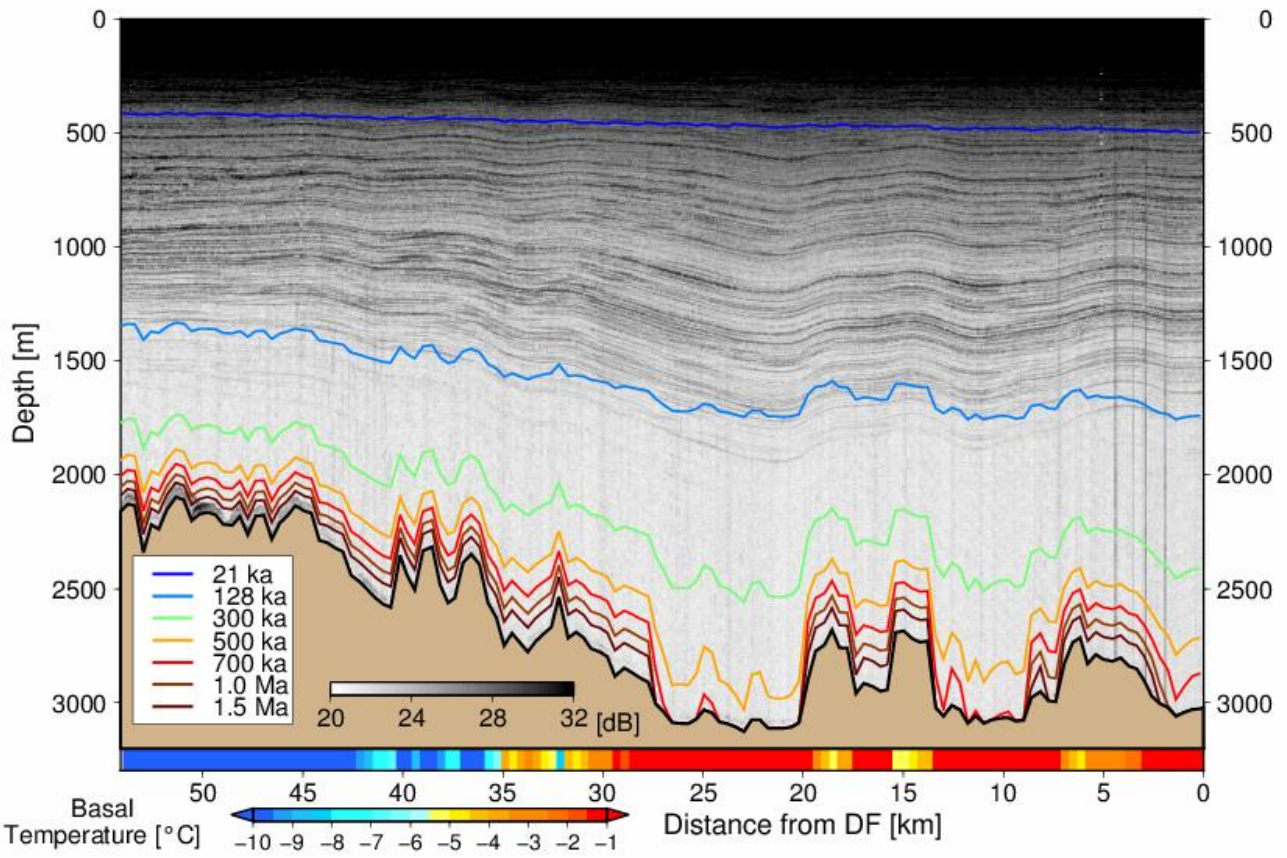


Fig. 15: Results of the experiments overlaid with the observed radargram for the DF–NDF transect. [A](#)

1014 combination of  $p = 3$  and  $\text{GHF} = 60 \text{ mW m}^{-2}$  is adopted in these experiments. The horizontal axis  
1015 indicates the distance from DF (km), and the vertical axis indicates the depth from the surface (m).  
1016 The gray coloring indicates the reflection intensity from the ground radar surveys, and the color  
1017 contours indicate the simulated age of the ice using the 1-D model. The bottom color bar indicates the  
1018 simulated basal temperature (relative to the melting point) at the present-day.